Materials for additive manufacturing

Article *in* CIRP Annals - Manufacturing Technology · June 2017

DOI: 10.1016/j.cirp.2017.05.009

CITATIONS
595

READS
10,210

7 authors, including:

David Bourell
University of Texas at Austin
230 PUBLICATIONS **7,782** CITATIONS
SEE PROFILE

Jean-Pierre Kruth
KU Leuven
343 PUBLICATIONS **35,033** CITATIONS
SEE PROFILE

Ming C. Leu
National Taiwan University
361 PUBLICATIONS **13,334** CITATIONS
SEE PROFILE

Gideon Levy
TTA Technology Turn Around
24 PUBLICATIONS **4,253** CITATIONS
SEE PROFILE

CIRP Annals - Manufacturing Technology 66 (2017) 659–681

Contents lists available at ScienceDirect

CIRP Annals - Manufacturing Technology

journal homepage: http://ees.elsevier.com/cirp/default.asp

Materials for additive manufacturing

David Bourell (2)[a,*], Jean Pierre Kruth (1)[b], Ming Leu (1)[c], Gideon Levy (1)[d], David Rosen [e], Allison M. Beese [f], Adam Clare [g]

[a] Mechanical Engineering Department, The University of Texas at Austin, Austin, TX, USA
[b] Department of Mechanical Engineering, KU Leuven, Leuven, Belgium
[c] Department of Mechanical and Aerospace Engineering, Missouri University of Science and Technology, Rolla, MO, USA
[d] TTA Technology Turn Around, Orselina, Switzerland
[e] George W. Woodruff School of Mechanical Engineering, Georgia Institute of Technology, Atlanta, GA, USA
[f] Department of Materials Science and Engineering, Pennsylvania State University, University Park, PA, USA
[g] Advanced Component Engineering Laboratory (ACEL), Faculty of Engineering, University of Nottingham, Nottingham, UK

ARTICLE INFO

Article history:
Available online 09 June 2017

Keywords:
Manufacturing
Material
Microstructure

ABSTRACT

Critical to the selection requirements for additive manufacturing (AM) is the need for appropriate materials. Materials requirements for AM include the ability to produce the feedstock in a form amenable to the specific AM process, suitable processing of the material by AM, capability to be acceptably post-processed to enhance geometry and properties, and manifestation of necessary performance characteristics in service. As AM has matured, specific classes of material have become associated with specific AM processes and applications. This paper gathers this information for each of the seven categories of ISO/ASTM AM categories. Polymers, metals, ceramics and composites are considered. Microstructural features affecting AM part properties are listed. Service properties of AM parts are described, including physical, mechanical, optical and electrical properties. An additive manufacturability index is proposed.

1. Additive manufacturing

Modern additive manufacturing (AM), also known as 3D Printing, dates to the mid-1980s. The first commercial AM fabricator, the SLA-1 was sold in 1988 by 3D Systems, founded in 1986. According to Bourell [38], precursor AM processes predate modern AM by about 30 years, with examples of lithographic human-scale manufacturing dating to the mid-1800s. Innovation here related heavily to process development as opposed to the creation and application of new materials. International popularity of AM skyrocketed beginning in 2009 due to multiple interrelated influences. These include the expiration of founding patents on AM fabricators, high-level governmental focus on AM as an advanced manufacturing process and the proliferation of low-cost AM printers based largely on material extrusion. This review follows a number of reviews in the CIRP Annals on the subject of AM [30,108,169,172,173,188]. The intent here is to focus on the materials used in AM processing, the issues defining the broad classes of material usage for AM processes and the general properties of specimens created using AM technologies. The focus is on manufactured parts intended for engineering service, for which considerations include stringent metrology, predictable mechanical properties and qualified microstructures. The scope includes bulk processing of materials in AM fabricators of the types commercially available. Micro/meso AM, bio AM and tissue engineering fall outside the scope of this work.

The joint ISO/ASTM terminology standard defines additive manufacturing to be the "process of joining materials to make parts from 3D model data, usually layer upon layer, in contrast to subtractive manufacturing and formative manufacturing methodologies" [143]. AM processes share the following commonalities: use of a computer to store and process geometric information and to drive the fabricator, and deposition of feedstock which is processed as points, lines or areas to create a part. The deposition volume element or voxel is small compared to critical features of the part. As such, AM processes do not require part-specific tooling.

2. AM processes

When considering commercially available AM fabricators, AM technologies are generally categorized into seven groups [143]. *Binder jetting* processes deposit liquid in the form of droplets to bind powder material. Often, the binder has adhesive qualities and is ink-jetted onto the surface of a powder bed. Production of structural materials typically requires some form of post-processing to remove the binder and to densify the constituent powder. *Directed energy deposition* (DED) is a collection of processes that use focused thermal energy to melt and bind materials fed in

* Corresponding author.
E-mail address: dbourell@mail.utexas.edu (. Bourell).

http://dx.doi.org/10.1016/j.cirp.2017.05.009
0007-8506/

powder or wire form. The thermal source is usually a laser or electron beam. These processes have the capability to produce large volume deposition rates (~cm^3/min) and are widely used to generate compositional gradients and for repair. *Material extrusion* is the most popular AM technology based on the number of fabricators and the low cost of the hardware. Feedstock is forced through a nozzle which defines the voxel size. In some instances, the feedstock is heated and melted prior to deposition. In other instances, the feedstock is deposited at room temperature, and a combination of solvent curing/drying and high-viscosity nature of the slurry serves to preserve part geometry. *Material jetting* is accomplished by selectively depositing droplets of material onto a build platform. Generally, current commercial material jetting technologies use photosensitive thermoset polymers which are cured upon deposition. This builds upon well-established inkjet technologies developed for conventional 2D printing. *Powder bed fusion* (PBF) entails surface exposure of a powder bed to a heat source to enable binding. The heat source is typically a laser or electron beam, although intensive light sources have been used with physical or chemical "masks" to allow all voxels on an entire surface to be processed simultaneously. Powder bed fusion, due to minimal constraints on feedstock type for manufacturing, is popular for part manufacture for service applications. *Sheet lamination* includes processes for which the feedstock is in the form of a sheet, which constitutes a layer in the build. The sheet is either cut to shape and then stacked/adhered to previous layers, or the sheet is bonded to the previous layer and then cut to form the layer geometry as well as hatched in the non-part area to facilitate removal of the part at the end of the build. *Vat polymerization*, the oldest of the commercial AM processes, involves photolithographic crosslinking of liquid thermoset polymer resins to form a solid.

3. Materials for additive manufacturing

For any manufacturing process, including AM technologies, the feedstock must be formed into a state compatible with the process in question (e.g., powder, sheet, wire, liquid). For example, in vat polymerization and photopolymer-based material jetting, the feedstock must be a liquid thermoset plastic monomer that will crosslink when exposed to the appropriate electromagnetic radiation.

Finally, the material must exhibit acceptable service properties to perform successfully in the given application. For the most stringent service applications, AM parts are usually post-processed in some fashion to improve the microstructure, reduce porosity and to finish surfaces, reduce roughness and meet geometric tolerance.

Table 1 lists the broad types of materials used in AM, by process category with commercial material entries. The plastics are listed as amorphous polymers, semicrystalline polymers and thermosets. Material extrusion uses amorphous polymers. The large viscous softening temperature range is helpful for successfully depositing the bead of plastic. Semicrystalline polymers typically soften over a very small temperature range with a dramatic change in viscosity. While this behavior is useful for powder bed fusion of plastics, the polymer flow characteristics are difficult to control using material extrusion. Chocolate is a special case and may be considered to be semicrystalline [55]. There are several chocolate printers based on material extrusion, but the present quality of multiple-layer parts is generally low, often limiting these fabricators to single layer deposition. Vat polymerization is limited to photosensitive thermosets. Efforts to mix particulate into the thermoset resin prior to processing were successful after silica nanoparticles became widely available, avoiding undesirable laser diffraction off the particles and settling of the nanoparticles so that periodic stirring of the resin was not needed [268,316]. Feedstock viscosity is also a concern in these processes, and particulate additions must not unduly hamper reflow into the processing region [180]. Material jetting typically uses photosensitive thermoset polymers. Particle additions to the resin prior to deposition are possible, but care must be taken to ensure resin viscosity remains low enough at the printing temperature for

Table 1
Current commercial materials directly processed by AM, by AM process category.

	Amorphous	Semi-crystalline	Thermoset	Material extrusion	Vat polymerization	Material jetting	Powder bed fusion	Binder jetting	Sheet lamination	Directed energy deposition
ABS [Acryonitrile Butadiene Styrene]	X			X						
Polycarbonate	X			X						
PC/ABS Blend	X			X						
PLA [Polylactic Acid]	X			X						
Polyetherimide (PEI)]	X			X						
Acrylics			X		X	X				
Acrylates			X		X	X				
Epoxies			X		X	X				
Polyamide (Nylon) 11 and 12		X					X			
Neat		X					X			
Glass filled		X					X			
Carbon filled		X					X			
Metal (Al) filled		X					X			
Polymer bound	X	X		X						
Polystyrene	X						X			
Polypropylene		X					X			
Polyester ("Flex")							X			
Polyetheretherkeytone (PEEK)		X		X			X			
Thermoplastic polyurethane (Elastomer)				X			X			
Chocolate		X		X						
Paper									X	
Aluminum alloys							X	X	X	X
Co–Cr alloys							X	X		X
Gold							X			
Nickel alloys							X	X		X
Silver							X			
Stainless steel							X	X	X	X
Titanium, commercial purity							X	X	X	X
Ti–6Al–4V							X	X	X	X
Tool steel							X	X		X

successful jetting [9,180]. Powder bed fusion of polymers is mostly limited to semicrystalline materials, but a few amorphous polymers such as polystyrene are processable. The difference in melt temperature on heating and the crystallization temperature on cooling should be large. By setting the fabricator part bed temperature between these values, it is possible to use the heat source, typically a scanning laser, to melt the polymer which cools but does not crystallize during the fabrication. This results in minimal in-build part distortion. For metal powder bed fusion, the general rule is that metallic alloys which are suitable for casting or welding can be processed successfully using AM. Part distortion can be severe and is controlled by a support structure during the build, managing cooling rates and careful design of laser scanning strategies. Binder jetting and some sheet lamination approaches rely on a binder to hold the part constituents together. In these cases, almost any feedstock may be used so long as it can be formed into powder or sheet. Ultrasonic consolidation is a sheet lamination technique that uses a sonotrode to ultrasonically weld metal foils in a layerwise fashion coupled to a machining head which forms part geometry. Directed energy deposition processes use metallic powder or wire feedstocks.

3.1. Plastics

3.1.1. Thermoplastics

Material extrusion and powder bed fusion and processes use thermoplastic polymers. Both involve thermal layer adhesion but exploit different mechanisms. For material extrusion, amorphous thermoplastics perform most suitably, while semicrystalline polymers are typically used for powder bed fusion.

3.1.1.1. Thermoplastics for material extrusion. For the material extrusion process, amorphous thermoplastics are preferred, due to their melt characteristics. These polymers, including popular ABS and PLA, soften over a wide range of temperature up to the so-called glazing temperature, forming a high-viscosity material ideal for material extrusion through a 0.2–0.5 mm diameter nozzle. Table 1 lists commercially available materials for material extrusion.

Material extrusion processes require supporting overhangs that must be removed by post processing. Two types are used: first, a lattice structure made from the same material but with a light design and low strength connection to the part and second, a more sophisticated approach requiring a two-head system with the support made from wax-based or poly-vinyl alcohol (PVA) materials. In the post processing stage, the supports are removed by melting or dissolving. PVA is used for PLA model materials and is a water soluble support material.

Typically, there are voids between the deposited tracks of extruded material. As a result, mechanical properties may be poor, and anisotropy effects are present.

3.1.1.2. Thermoplastics for powder bed fusion. Powder bed fusion uses an IR laser (typically a 10 μm CO_2 laser) or an IR or UV heat source (lamps) for melting and fusion of mostly semicrystalline powder feedstock. The thermal behavior of the most popular semicrystalline material for powder bed fusion, polyamide 12 (nylon), is depicted in Fig. 1. The melting point is about 35 °C higher than the crystallization temperature. By setting the AM fabricator temperature between these peaks, material melted by the laser remains molten and in thermal equilibrium with the surrounding unmelted powder. Recrystallization eventually occurs uniformly after the build, minimizing creation of residual stresses.

The powder bed fusion process does not require supports for overhangs in the case of plastics due to the support provided by the surrounding powder cake. The build can include multiple nested parts. Almost completely dense, low porosity objects are obtained by adjusting processing parameters. For liquid pressure tight applications, a post infiltration is required [256].

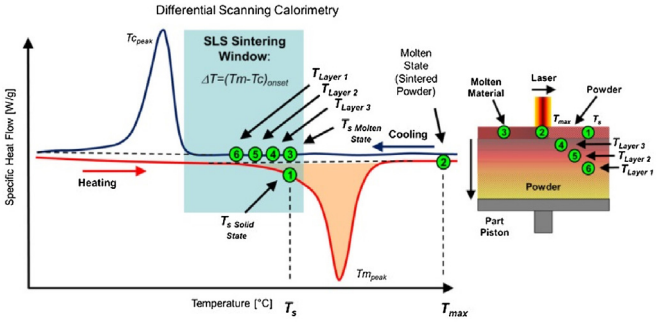

Fig. 1. A typical DSC scan for semicrystalline polyamide [13].

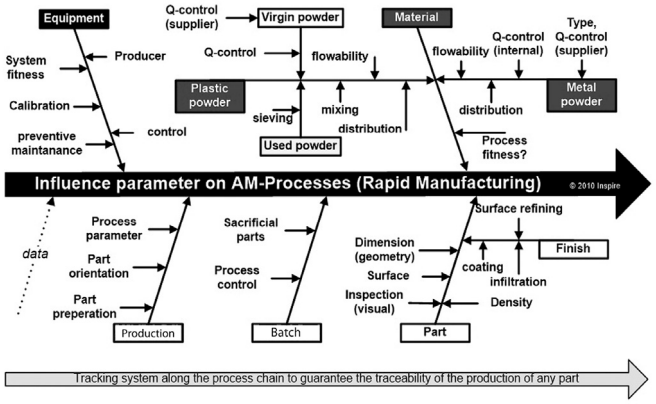

Fig. 2. Ishikawa diagram that presents the interdependency of the main intrinsic and extrinsic properties that define the suitability of a material for powder bed fusion.

Feedstock preparation is complex when controlled properties and structure are desired [14,254,255] and imposes additional requirements beyond the basic, essential thermal behavior. The material must be pulverized. Pulverization can be achieved by dissipation, cryogenic grinding or coextrusion of non-miscible polymers. Powder bed fusion feedstock characteristics are depicted in Fig. 2.

Resolution depends primarily on the CO_2 laser spot size and the galvanometer deflection angle which defines the apparent spot size and location in the XY plane. Surface quality is influenced by the outline-scan processing parameters, scan speed, the layer thickness and particle size. Dimensional accuracy is negatively impacted by thermal dilatations, since the surrounding unmelted powder ("part cake") is hot.

Thermally-induced extension of molecular chains during processing results in a gradual increase of melt viscosity which is deleterious to successful powder bed fusion processing, eventually resulting in the so-called "orange peel" effect on part surfaces. Strict powder recycling management is essential to prevent this. Powder blends are produced by mixing 30–50% fresh powder with mixtures of overflow powder and part cake to optimize recyclability and feedstock performance. On the other hand, the molecular weight increase leads to parts with enhanced mechanical properties and strong interlayer bonding [14].

Efforts to increase productivity concentrate on replacing the laser as the energy source with a process that processes the entire layer simultaneously. Examples are High Speed Sintering and Multi Jet Fusion™ that utilize an IR absorber powder deposited selectively coupled to an IR area heating source [138]. An alternative is use of thermal print heads as is embodied in Selective Heat Sintering™ technology [33].

3.1.2. Thermosets

Typical photopolymer materials used in AM are composed of monomers, oligomers, photoinitiators, and a variety of other additives including inhibitors, dyes, antifoaming agents, antiox-

idants, toughening agents, etc. that help fine-tune the photopolymer's behaviors and properties [116]. The first photopolymers used in vat photopolymerization were mixtures of UV photoinitiators and acrylate monomers [146]. Vinylethers were another class of monomers that were used in early resins. Acrylate and vinylether resins exhibited considerable shrinkage, from 5 to 20% [65], which caused residual stresses to accumulate as parts were built layer-by-layer which, in turn, caused significant warpage. Another disadvantage of acrylate resins is that their polymerization reactions are inhibited by atmospheric oxygen. To overcome many of these disadvantages, epoxies were introduced in the early 1990's and brought significant advantages to the vat photopolymerization process, but complicated the formulation of resins.

Epoxies are common cationically polymerized photopolymers. Epoxy monomers have rings which, when reacted, open to provide sites for other chemical bonds. Ring-opening is known to impart minimal volume change, because the number and types of chemical bonds are essentially identical before and after reaction [146]. As a result, epoxy SL resins typically shrink less than acrylates and have much less tendency to warp and curl. Almost all commercially available SL resins have significant amounts of epoxies.

A photopolymerization reaction takes place in several steps, as shown in Fig. 3. First, the photoinitiator, denoted P-I, is activated upon exposure to radiation within an appropriate wavelength range. Second, the reactive portion of the photoinitiator reacts with a monomer molecule, M, to form a free radical, $M^{\bullet}$. Third, the propagation step forms long polymer chains and also causes chains to crosslink. The fourth step is termination, where polymerization comes to an end, usually by one of three mechanisms, including recombination (two chains combine), disproportionation (cancelling of one radical by another without joining), or occlusion (free radicals become trapped by the polymer network).

Cationic photopolymerization proceeds in a similar manner, with the differences compared to the free radical kind being a different photoinitiation mechanism and a cationic initiator used to transfer the charge to a monomer (instead of an anion).

Broadly, the polymer classes that are cationically polymerized include olefins with electron-donating substituents and heterocycles, of which epoxy is an example (heterocycle = cyclic monomer where not all atoms in the cycle are carbon). A typical catalyst for a cationic polymerization is a Lewis Acid, such as BF_3 [312]. Interest in cationic photopolymerization accelerated with the development of the epoxy-based photoresist SU-8, which is commonly used in the microelectronics industry.

Commercial AM resins are mixtures of acrylates, epoxies, and other oligomer materials. Acrylates tend to react quickly, while epoxies provide strength and toughness to the solid [32]. Acrylates polymerize radically, while epoxides polymerize cationically to form their respective polymer networks. The two types of monomers do not react with one another but, since they are mixed, form an interpenetrating polymer network (IPN) upon reaction [66,78]. IPNs are a special class of polymer blends in which both polymers generally are in network form [79,263,264], and which are originally generated by two concurrent reactions instead of by a simple mechanical mixing process.

The acrylates and epoxies affect each other physically during the curing process. The reaction of acrylates will enhance the photospeed and reduce the energy requirements for the epoxy reaction. Also, the presence of acrylate monomers may decrease the inhibitory effect of humidity on epoxy polymerization. On the other hand, the epoxy monomer acts as a plasticizer during the early polymerization of the acrylate monomer; the acrylate forms a network while the epoxy is still in a liquid stage [79]. This plasticizing effect, by increasing molecular mobility, probably favors the chain propagation reaction [80]. As a result, the acrylate polymerizes more extensively, resulting in higher molecular weights in the presence of epoxy than in the neat acrylate monomer. Furthermore, the acrylate exhibits a reduced sensitivity to oxygen in the hybrid system than in the neat composition due to the viscosity rise caused by epoxy polymerization, which may result in reduced diffusion of atmospheric oxygen into the material [79].

$$P\text{-}I \rightarrow \text{-}I\bullet \quad \text{(free radical formation)}$$
$$I\bullet + M \rightarrow I\text{-}M\bullet \quad \text{(initiation)}$$
$$I\text{-}M\bullet \rightarrow \ldots \rightarrow I\text{-}M\text{-}M\text{-}M\text{-}M\ldots\text{-}M\bullet \quad \text{(propagation)}$$
$$I\text{-}M\text{-}M\text{-}M\text{-}M\ldots\text{-}M\text{-}I \quad \text{(termination)}$$

Fig. 3. Free radical photopolymerization procedure.

Some example resin formulations will be covered here that are taken from representative patents [110,190,216]. Of those formulations that contain both free radical and cationic photopolymerizable components, both monofunctional and higher functionality monomers are used typically in vat photopolymerization resins [110,190]. (Meth)acrylates and poly(meth)acrylates are typical and denote an acrylate, a methacrylate, or a mixture. Example commercial monofunctional monomers include alkyl (meth)acrylates SR 313A and 31313 from Sartomer Co, and Ageflex FM6 from Ciba Specialty Chemicals. Polyfunctional (meth)acrylates often have glycol or bisphenol groups and can be di-, tri-, tetra-, or pentafunctional. Example commercial compounds include SR 238, SR 350, SR 454, SR 8335, among others, from Sartomer Co. A free radical photoinitiator component must be included and is often a benzoin, acetophenone, benzyl ketal, cyclohexyl phenyl ketone, among others, for UV curable formulations. Other appropriate photoinitiators are available that enable visible light curing.

For the epoxide cationically initiated component, a very wide variety of compounds can be used, as is evident in the patent literature. Categories of suitable compounds include polyglycidyl and non-glycidyl epoxy compounds, and epoxy phenol novolac compounds. Functional groups capable of reacting via a ring-opening mechanism are almost always used. Examples include oxirane-(epoxide), oxetane-, tetrahydrofuran- and lactone-rings. For several years, oxetane-containing stereolithography (SL) compounds were marketed aggressively due to the favorable mechanical properties of resulting resins. Suitable cationic photoinitiators, activated by UV radiation, include onium salts, metallocene salts.

Toughening agents are used frequently in commercial resins to improve mechanical properties of fabricated parts. Such toughening agents may be reactive or non-reactive and may be in the form of a phase separating liquid or particles. In one embodiment, the particles have a crosslinked elastomeric core and a shell containing reactive groups [216]. Example core materials include polysiloxane, polybutadiene, rubber, or other elastomers, while example reactive shells include compounds with epoxy, oxetane, hydroxyl, vinyl ester, vinyl ether, or acrylate groups, or mixtures of these.

Resin formulations have suffered from two primary drawbacks that have prevented their more widespread usage as production materials: sensitivity to water/humidity and tendency to age. Several research groups have characterized mechanical properties of SL resins and their changes over time under a variety of environmental conditions [208,235,244].

Large Area Maskless Photopolymerization (LAMP) utilizes a silica nanoparticle composite photopolymer intended to fabricate integral ceramic cored molds for casting aerospace parts, including turbine airfoils [315]. Since they intend to fabricate molds directly, they desire a very high silica loading in the resin. Their resin consists of ethoxylated penta erythryitol tetraacrylate, a small amount of hexanediol diacrylate (HDDA), and 55 volume percent of silica (~72 weight percent). Experiments demonstrated excellent curing, with 75% degree-of-cure readily achieved.

Thermoset materials for jetting processes have formulations that are described similarly to vat photopolymerization formulations. Patents describing these materials use similar categories, but typically do not identify free radical and cationic reactions as separate categories [225]. The patents identify photopolymerizable mixtures and their photoinitiators, but lump together acrylate

and epoxy compounds and their photoinitiators. They do, however, typically discuss resin viscosity carefully since deposition through ink-jet nozzles is a critical element of their usage in manufacturing equipment. These resins are typically formulated to have viscosities greater than 50 cP at room temperature, but below 15–20 cP at an elevated temperature. Commercially available ink-jet deposition heads are advertised as being capable of printing many liquids with viscosities up to 40 or 50 cP. However, in practice, the resin should have a viscosity less than half of the advertised maximum to ensure clog-free operation. Material jetting machines have heaters that deliver heated liquid to the deposition heads, which enables the ejection of materials that have high viscosities at room temperature.

One of the advantages of material jetting processes is the capability to deposit multiple materials, for example, having different banks of nozzles depositing different materials. If these multiple materials are deposited in the same layers, then the resulting solid can exhibit mechanical properties that are intermediate to the properties of the constituent materials.

Researchers have characterized mechanical properties of material jetted parts. Results indicate that parts have considerable variability in tensile and compressive properties [221] and exhibit anisotropy. Interestingly, this anisotropy does not result in the weakest properties when the test direction is parallel to the build direction (Z orientation), but rather at a test direction between 40°–60° along the XZ direction. The authors hypothesize that shear along the build plane has a more significant effect on properties than tension orthogonal to the build plane [221]. Others have characterized part property changes over time and demonstrated the effects of aging [31].

3.2. Metals

Powder bed fusion and directed energy deposition are the main powder-based AM processes that are commercially used to manufacture quality metal parts. A metal wire feed can also be used instead of powder feed in DED. Binder jetting is also used to produce metal parts. Polymer matrix parts are made that need furnace de-binding and sintering and/or infiltration with a lower melting point metal (e.g., brass) to obtain dense metal parts.

The set of common commercially available alloys is limited to pure titanium, Ti6Al4V [41,97,282,330], 316L stainless steel [227, 324,328], 17-4PH stainless steel [223,265,267,323] and 18Ni300 maraging steel [49,158], AlSi10Mg [42,44,156,210], CoCrMo [292,319], and nickel based superalloys Inconel 718 and Inconel 625 [15,85,198,237]. This range is continually expanding with new entrants to the materials supply market. Precious metals such as gold, silver or platinum have been processed indirectly by 3D printing of lost wax models, but are currently also being directly used in selective laser melting (SLM) [159,345]. Several factors contribute to this limited metal palette. When fusion is involved, the metals generally must be weldable and castable to be successfully processed in AM. The small, moving melt pool is significantly smaller than the dimensions of the final part (typically on the order of 10^2–10^4 times smaller). This local hot zone in direct contact with a large and colder area leads to large thermal gradients causing significant thermal residual stresses and non-equilibrium microstructures. For powdered feedstock, particles should preferably be spherical with a certain size distribution, which is different for PBF and DED. The latter tends to be less sensitive to the dimensional qualities of the feedstock. A wire is also a suitable precursor material for certain DED processes, creating a larger melt pool than powder based DED allowing a higher production rate [89].

3.2.1. Material related challenges in metal AM

i) Affinity for atmosphere constituents

Powder particles of Al and Al alloys have a stable Al_2O_3 layer at their surface, hampering particle sintering or melt coalescence.

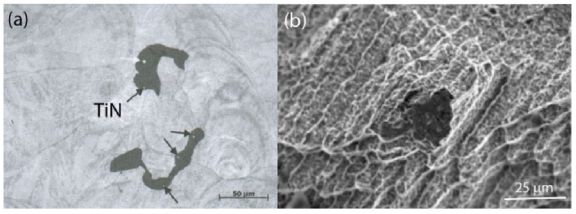

Fig. 4. (a) Large dark grey oxide particles and small TiN particles indicated by the arrows, trapped inside 18Ni300 SLM part [281]. (b) Fracture surface of a DED Inconel 718 part having an Al_2O_3 particle inclusion [340].

This has a negative effect in electron beam melting (EBM) where the powder bed needs to be pre-sintered to slightly bind the powder particles together before melting them. This is needed to avoid repelling of powder particles due to the negative charge induced by the electron beam, causing the particles to be ejected from the powder bed. 18Ni300 maraging steel and Inconel 718 form stable oxides during processing that float to the top of the melt pool [281,340]. Addition of a new layer will break these oxides and hereby move the majority of them to the new formed top surface, but some particles can stay behind in the solidified microstructure. These brittle particles act as stress risers and are detrimental to mechanical properties, Fig. 4. In the case of materials for which the reaction with oxygen is very exothermic, (e.g., Mg), AM can even be very dangerous if not performed in an oxygen free atmosphere [226].

Higher levels of oxygen in Ti6Al4V increase the strength but reduce the ductility [272,300]. Care must be taken to minimize the oxygen, nitrogen or moisture, as it may decrease mechanical properties and powder recyclability.

ii) High reflectivity and thermal conductivity

Creating an effective melt pool is difficult for alloys that have a high reflectivity (hence low absorption) and high thermal conductivity, such as copper [241,248], aluminum, silver and gold [159,251,345]. High power lasers up to 1 kW have been used to process these materials, along with different wavelengths to increase the laser absorption (Fig. 5) [35]. Powders do scatter and entrap the laser light and are two to seven times more efficient to absorb the laser light compared to flat surfaces [162].

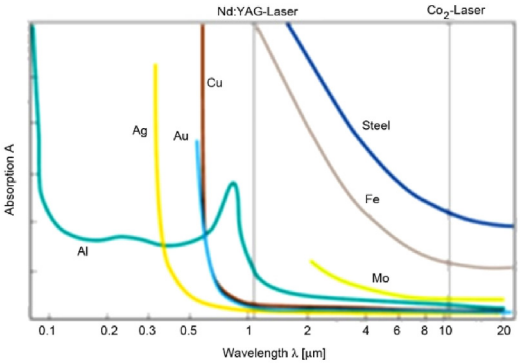

Fig. 5. Absorption of several pure metals at room temperature, for different wavelengths [35,150].

iii) Residual stress

In general, AM residual stress distributions feature high tensile stresses at outer surfaces, balanced by a large zone of compressive stresses in the center, as illustrated by the stresses in an Inconel 718 block produced by laser metal deposition (LMD) and shown in Fig. 6 [249]. Stress gradients also develop in the build direction depending on the part geometry, height of the part, and connection

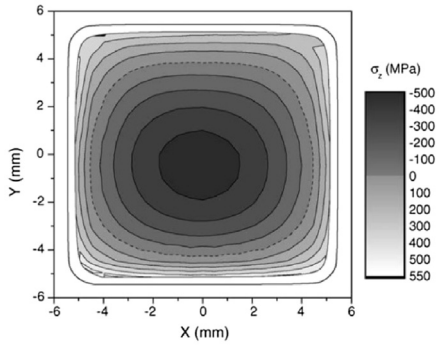

Fig. 6. 2D map of the vertical residual stresses at midheight of a 100 mm high Inconel 718 pillar structure made by LENS [249].

method to the base plate; thus modeling and experimental quantification of residual stresses is necessary in AM for their mitigation [215,306,307].

While deformations due to residual stresses are a general phenomenon, the occurrence of cracks and the type of cracks are material dependent. For example, if they crack, Ti6Al4 V (that is less prone to cracking) and M2 high speed steel (that is more prone to cracking) develop macroscopic cracks [157]. On the other hand, several nickel based alloys exhibit microcracking, in particular those with a high Al and Ti content as vital elements for formation of γ' precipitates [91]. Microcracks are caused by local influences around the melt pool such as liquation of low-melting point phases at the grain boundaries, local aging and embrittlement in the heat affected zone (HAZ), or solidification cracking when remaining liquid zones act as crack initiation sites in the almost solidified melt at the end of solidification [48]. Inconel 625 achieves its hardness by solid solution strengthening, and Inconel 718 only has a moderate content of γ' precipitate forming elements, and these alloys are readily processed by AM [15,198]. Inconel 738LC forms extensive γ' in the HAZ, embrittling the material, leading to crack formation [177,250].

3.2.2. Microstructure

A small melt pool size and high cooling rate determine the unique microstructure of the produced parts. The most important solidification factors are the temperature gradient in the liquid GL, solidification rate R, undercooling of the liquid phase and alloy constitution. GL and R vary along the melt pool boundary, but it can be stated that the temperature gradients GL can reach values up to 10^6 K/m for SLM [280]. The stability of the solidification front determines the type of microstructure. For pure metals that have a single melting temperature, the stability is only determined by the thermal gradients in the melt. Depending on the sign of GL, either a planar solidification front or an unstable solidification front may occur. Nevertheless, in metal AM processes, heat is applied to the melt pool and therefore GL is always positive. Alloys, on the other hand, have a solidification range rather than a specific melting point, which causes alloy elements to redistribute between solid and liquid. The compositional gradient leads to a gradient in the effective liquidus and solidus temperature, an effect known as constitutional undercooling [168]. Even though GL is positive, constitutional undercooling may destabilize the planar front causing cellular-dendritic solidification [278].

In the planar solidification mode, the grains for which the easy growth direction is closest to the direction of heat flow will grow the fastest via a process known as competitive growth. Although heat may flow from the melt pool to the sides, it is mainly conducted towards the cooler material underneath and the baseplate, although this varies with build height and part geometry. The preferential growth direction for cubic crystals is the <100> direction, and <10$\bar{1}$0> for hexagonal crystals. For a cellular-dendritic solidification mode, the cells also grow along the easy growth direction, but it does not necessarily have to be aligned with the maximum heat flux.

Microstructures obtained after AM can generally be classified into two categories: those that form a columnar microstructure and those that solidify in a cellular-dendritic regime. The most important material in the first category is Ti6Al4V [154,282], although columnar growth has been observed for other materials (such as Inconel 718, Ta and W) as well [237,280,302]. Despite the significant alloying content of a combined 10 wt% of Al and V, the solidification range of Ti6Al4V is less than 10 K [295], and partitioning of alloy elements and related constitutional undercooling is limited. This results in vertical β grains growing across many layers, which transform to α' martensite during quenching for SLM and lamellar $\alpha + \beta$ for wire EBM. In DED, the microstructure varies between that in SLM and EBM, and displays a gradient between part bottoms and tops. Fig. 7a shows the typical columnar prior β grains that contain the acicular martensite obtained after SLM. In the absence of the β to α or α' transformation, Ti6Al4V would display an extreme <100> texture like Ta [280], but the 12 crystallographic variants of the β to α transformation lead to a weaker texture.

Most other materials solidify in the cellular-dendritic regime. The melt pools were invisible for Ti6Al4V, but are clearly delineated for other materials, shown for 316L in Fig. 7b. Notable examples are AlSi10Mg, 316L, 18Ni300 maraging steel and Inconel 718. In the side views of the microstructures of these materials as shown in Fig. 8 [302], the red arrows indicate former melt pool boundaries. The inserts on the top right of each image shows a cellular structure of a strikingly same size for all materials. For AlSi10Mg, the intercellular zone consists of an Al–Si eutectic, but for all other materials, the contrast is provided by a small amount of microsegregation. All cubic materials in this category also develop a <100> texture in the building direction, although it is not as strong compared to the columnar microstructures [72,279].

The fine scale of the cellular structure is due to the high cooling rates during metal AM manufacturing, which can reach 10^6 K/s in SLM [280]. As a result, the microstructure after SLM and DED is fine and saturated with alloy elements, dislocations and metastable phases [151]. This is different in the EBM process in which high preheating temperatures provide a stress relief and in-situ annealing leading to coarser structures [56]. The fine micro-

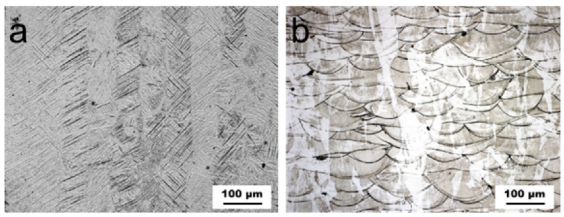

Fig. 7. (a) The columnar microstructure in SLM of Ti6Al4V [300] and (b) the visible melt pools in SLM of 316L. The building direction for both images is vertical and upwards (Source: KU Leuven).

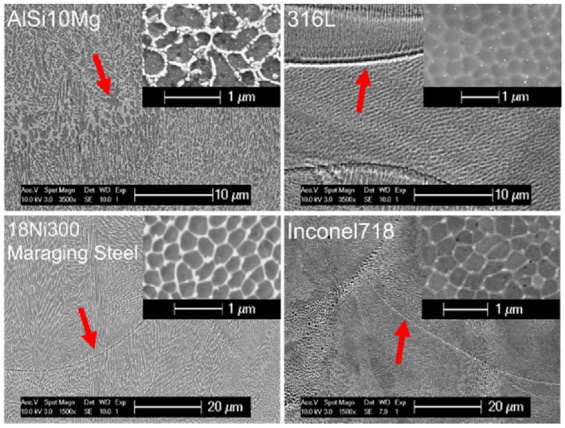

Fig. 8. Side views of the cellular microstructure of common SLM produced materials. The insets are close-ups of the top view [302].

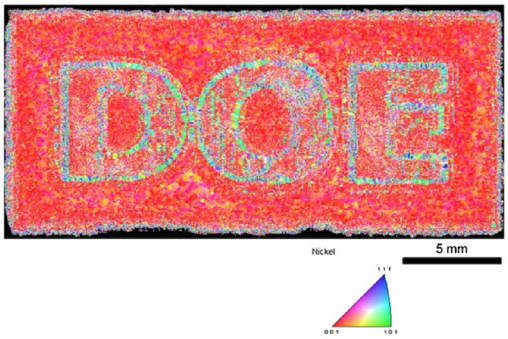

Fig. 9. Local texture control by manipulation of the process parameters, illustrated by electron backscatter diffraction crystal orientation mapping of Inconel 718 [85].

structures cause strengths comparable to wrought or cast material, sometimes even approaching the strength of conventional material in the age hardened condition (e.g., AlSi10Mg) [43]. As a trade-off, the ductility is often lower [103,301]. This is especially the case for Ti6Al4V, for which extensive research effort has focused on improving the ductility, either by post-process heat treatment [103,296,301] or manipulation of process parameters [318,321]. Hot isostatic pressing (HIP) also improves fatigue properties [186,318].

Texture can be manipulated by variation of the rotation of the scan pattern between layers by changing the conditions for competitive growth [279]. Recently, however, the ability to change the solidification mode for one material by changing the process parameters has also been developed [227,237]. Through variation of the scan speed and laser power, researchers at Oak Ridge National Laboratory were able to change between planar, cellular-dendritic and a mixed solidification mode [85]. This created a substructure shown in Fig. 9 which was invisible to the naked eye, but made visible via electron backscatter diffraction (EBSD) imaging of the crystal orientations.

3.3. Ceramics

Several reviews of AM of ceramics have been published [83,84,108,130,247,286,290,311]. Ceramics, due to their combination of high melting point and low toughness, are difficult to process directly in AM [62]. Alumina and its alloys have been directly processed using directed energy deposition [29,231,232] and powder bed fusion [128,311], but full density processing is difficult. In most cases, attempts to direct process ceramics have resulted in thermally induced cracking. Approaches to mitigate cracking include process optimization, adding auxiliary devices (ultrasonic, thermal, magnetic) and a doping toughening approach [231]. Process optimization for directed energy deposition of crack-free alumina includes high scan speed exceeding 700 mm/min [231].

Indirect AM processing of ceramics requires use of a binder in some form that holds the part together after AM. With the exception of directed energy deposition, all categories of AM have been utilized in creation of indirect AM ceramic parts [108]. Early attempts based on material extrusion include Fused Deposition of Ceramics invented at Rutgers University [6,211,213] and Robocasting, developed at Sandia National Labs [51,52,53,54]. In the mid-1990s sheet lamination methods were used for processing alumina/zirconia [121], silicon carbide [163] and silicon nitride [164,165,242].

Another early approach involved mixing fine ceramic particulate, typically alumina or silicon nitride, into a stereolithography resin [123,131,135,315]. Optoforming is a variation which uses a more aggressive mechanical resin spreading mechanism [28]. The particulate must be fine to allow a non-settling suspension to be made. It must have an index of refraction close to the polymer resin to prevent unwanted diffraction [131]. The particulate wavelength absorption edge should be less than the wavelength used for

Fig. 10. Parts fabricated from alumina paste using the Ceramic-On-Demand Extrusion process [115].

crosslinking. Finally, the solids loading must be less than about 50% to maintain a flowable viscosity for the resin.

Typically the binder for indirect AM of ceramics is transient in nature, being converted or removed in a post-processing step such that the final part is a neat ceramic or a ceramic composite. With powder bed fusion processes, both mixed powder/binder systems [e.g.,83,259] and slurry approaches [277] have been used. Ceramic AM parts may be post-infiltrated to create full density parts in lieu of high-temperature furnace post-sintering [100–102].

Freeze-form Extrusion Fabrication (FEF) is an environmentally conscious AM process that builds 3D ceramic parts in green state layer-by-layer by computer controlled extrusion and deposition of aqueous colloidal pastes (with a trace amount of organic binder) [141,185,194,195]. Unlike robocasting [189] which uses a hot plate for depositing aqueous ceramic pastes, FEF fabricates ceramic parts by depositing aqueous pastes under controlled freezing conditions, thus enabling the building of relatively large parts. However, a major issue of the FEF process is that sizable ice crystals may form during paste freezing, which may result in significant pores and reduced part density after part sintering. To overcome this issue, the Ceramic-On-Demand (CODE) process, which is a room-temperature, extrusion-based AM process that applies radiation heating for uniform drying of paste between successive layers, has been developed recently and shown to be capable of producing complex ceramic parts (Fig. 10) with near theoretical density and highly packed microstructure [115,212].

A more detailed recent review of AM ceramic processing is found in [108].

3.4. Composites

Composite development takes into consideration the following factors: feedstock material and preparation (molten, filament, fibrous, particulate), homogeneity and properties. It is vital that the interface between the matrix and the dispersed or embedded phase be engineered for proper bonding, transfer of load and protection against corrosion. Under consideration here are composites fabricated by additive manufacturing without post-processing such as infiltration or coating [21,289].

3.4.1. Polymer composites

Material extrusion processes allow for discrete, heterogeneous layering of a material for a laminate composite. The feedstock may alternatively be formulated prior to deposition for a matrix composite [99,253]. Additives to polymer feedstock must be of the proper composition to yield an extrudate that is of low enough viscosity to deposit and provide strength over the entire part build time. Feedstock often consists of the matrix polymer, tackifier, plasticizer, surfactant, and secondary phases such as particulates or fibers of metal, ceramic or polymer composition. Tackifiers provide flexibility, plasticizers improve rheology, and surfactants change dispersion character of the secondary phase [142,175]. Polymer composites with dispersed nanotubes have been achieved by formulating operational feedstock [99,243,253]. Fiber reinforced composites, usually carbon fiber reinforced composites or fiberglass, vary in mechanical properties depending on orientation of fibers; whether the fibers are whiskers (<50 μm), short (>50 μm), or continuous (full length of the component); and matrix-fiber interface design [303]. A commercial example of AM fiber

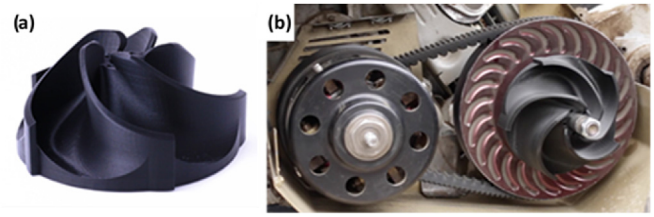

Fig. 11. (a) Chopped micro-carbon reinforced nylon impeller. (b) Engine mounted Onyx impeller in forced-air cooling application [209].

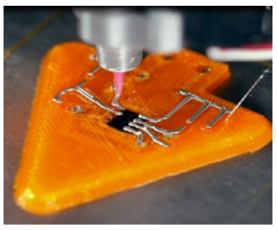

Fig. 12. PLA component with 3D silver circuitry via FDM [299].

reinforced composites is the Markforged© Mark series benchtop machines, which are capable of embedding continuous carbon fiber, chopped carbon fiber, Kevlar, and fiberglas in a nylon matrix; mechanical testing has suggested a higher strength-to-weight ratio than 6061-Al alloy for continuous fiber composites. The Onyx filament contains chopped micro-carbon fibers, combing the toughness of nylon and thermal properties of carbon. This composite filament provides a dimensionally stable, stiff, and heat tolerant engineering material with high quality surface finish, Fig. 11 [209].

Benchtop 3D printers are now available for electronics development (Fig. 12). This printer uses PLA filament and highly conductive, colloidal, silver ink to inlay 3D circuits into fully functioning components without further processing. Software enables a pause in fabrication to insert pre-made components. Inks have been developed that are 20,000 times more conductive than commercial conductive thermoplastic filament [299].

Powder bed fusion is another popular approach for composite materials research development, notably due to the relatively large number of fabricators. Liquid phase sintering (LPS) of the matrix is enabled via the secondary phase and the ability to pre-mix powders for additional property benefits. LPS is often used for polymer-matrix composites in the production of bioactive materials (Fig. 13), e.g., polyetheretherketone (PEEK)/hydroxyapatite (HA) [276], polycaprolatone (PCL)/HA [313], tricalcium phosphate (TCP)/poly-L-lactic acid (PLLA) [200], and PCL microspheres + HA/PCL [93]. Particulate and whisker reinforced polymers of many chemistries have been processed, including glass [57,59], nano-clay [161], or silica in nylon [60]; carbon fiber [119], silicon carbide [117], or potassium–titanium whiskers in polyamide [331]; nano-alumina in polystyrene [343].

Vat polymerization has been used to process bioactive glass scaffolding [98], randomly oriented graphene oxide reinforced

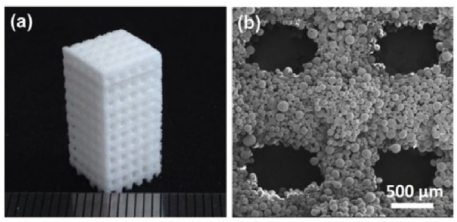

Fig. 13. (a) Sintered scaffold (8.8 × 8.8 × 18.4 mm) with highly ordered cuboid morphology. (b) SEM magnified image within pores [93].

thermoplastic [199], multi-polymeric microstructural arrays, or laminates with various surface properties [297]. Using oxygen-inhibition lithography (OIL), the dimensions of fine structures are not limited by UV exposure, but by the volume of material allotted for construction of each layer and the photomasking detail. OIL can be used to easily fabricate structures from multiple resins with differing chemical characteristics to generate a laminate structure.

3.4.2. Metal composites

Metal-matrix composites fabricated using AM include particulate composites, fibrous composites, laminates and functionally gradient materials (FGMs). SLM and laser metal deposition (LMD) are highly favored processes for AM of metallic materials.

It is possible to fabricate metallic composites from powder precursors by liquid phase sintering (LPS) to bind the matrix material and secondary phases [126]. This technique has been applied to metal-matrix composites (MMCs) for full consolidation and improved sinterability. In the case of WC-Co/Cu composites, with WC particulates reinforcing the Co matrix, bronze (Cu–Sn) or copper additive is used for LPS [173]; other additives such as lanthanum oxide can be used to decrease surface tension to improve densification [125]. Additives to control grain growth, improve sinterability, and adjust the coefficient of thermal expansion (CTE) are critical for processing of FGMs. These are particulate composites which grade across a part through more than one material with control of anisotropic response [95,160]. FGMs have been graded from metal to metal and from metal to ceramic, using powder precursors. An example of metal-to-metal gradient may be seen in Fig. 14 [325,339]. Using direct metal deposition (DMD or metal DED) of materials with similar thermal expansion coefficients, the gradient is possible without stress fracture, as in grading from stainless steel to Inconel 625 [46].

DMD techniques have also been applied to metal matrix composites with ceramic reinforcing phases, e.g., Ti6-4/TiB [304], Ti6-4/TiAl [113], Ti6-4/Ni [341], Ti6-4/WC [106,107], W-Co cermets [320], Ti/SiC [73,74], TiC/Ni/Inconel [342], Inconel/WC [3,4] and quaternary metal matrix reinforced with borides [224].

Graded materials for seamless and limited stress junction of multiple materials are highly favorable in aerospace applications, which may require different mechanical and thermal properties within a single component, such as a propulsion nozzle [136]. Grading two alloys is a very good way to complement the properties of two metals that may be incompatible due to their different CTEs. For example, a stainless steel alloy (304L) has been graded to a nickel-rich alloy (Invar 36) with a low CTE for a mirror surface, without fracture or warpage due to their CTE difference [136].

Laser techniques can also be used to form composites by in-situ reactions. The laser can be used to compensate activation energy required to form new compounds, or trigger a chemical reaction by providing the necessary thermal energy to propagate a reaction [113,183,261].

Ultrasonic consolidation (UC) can be used as a solid-state fabrication process to join layers of metal foils into a 3D structure

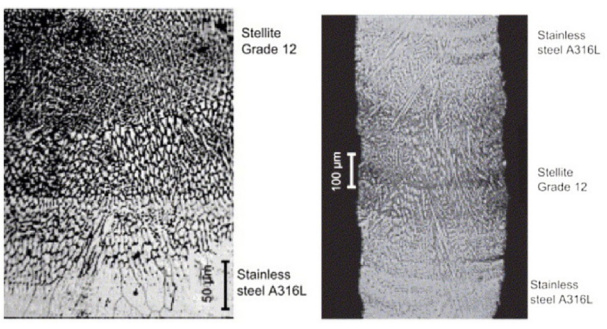

Fig. 14. Gradient from Stellite 12 to A316L via laser powder deposition [325].

followed by a sequential machining step to form the geometry. Fibers have been embedded in metal matrices during the UC process, making it a strong candidate for fiber reinforced metallic composites [327]. Fabrication of complex geometries with high accuracy is a major advantage of UC processing. Because this technique does not reach high temperatures ($<T_m/2$) and there is no melting, there is no dimensional error due to shrinkage or residual stress from cooling as is the case for melting-based processes. Successful lamination has been demonstrated to embed SiC fibers in an aluminum alloy matrix, embed sensors [193], and fabricate composites of aluminum alloy and stainless steel, Fig. 14 [149]. Despite the advantages of UC, consideration for design of the material interface is still crucial to prevent defects which will ultimately reduce the mechanical advantage of the embedded phase.

3.4.3. Ceramic matrix composites

Biomaterials is a major area driving AM research and development in AM of ceramics [77,109,270,283,308]. Select biomaterial scaffolds of ceramic in polymer require no sintering or post treatment and are effectively available for use immediately after fabrication [93,200,276,313]. Much like the biopolymer composites, the bioceramic composites are particulates blended for homogeneity and then consolidated via selective laser sintering (SLS) or some other AM process.

Binder jetting may also be used to produce other ceramic matrix composites. Binder jetting allows for dimensional accuracy and complex geometry; overhangs, arches, and cellular structures are possible due the support of the powder bed. Conventionally manufactured composites of silicon carbide or SiC reinforced composites require post processing to introduce carbonaceous feedstock or molten silicon for a reaction bonded SiC. Via binder jetting and preparation of the powder bed composition, the fabrication of Si-SiC composites has been demonstrated. These composite structures are sintered to near net-shape. The ability to create a composite preform allows a high degree of control of the final sintered ceramic composite [111].

The application of ceramic suspensions provides a better solution for controlled processing of dense components where traditional processing knowledge can be applied. Advances have been made to consolidate opaque suspensions in stereolithography [346]. High solids loading suspensions using UV curable polymer surfactants were demonstrated on alumina/zinc oxide (Al_2O_3/ZnO) composites [75].

A unique AM process that combines ceramic sol–gel processing and SLS is selective laser gelation (SLG). Effectively the same mechanical process as SLS, SLG utilizes the gelation of a sol to entrap suspended particles in a matrix. This technique capitalizes on the use of gelation so, unlike SLS, it requires less energy for consolidation. Also, the gelation mechanism allows flexibility and application to slurries; one such example is silica sol with embedded stainless steel [201].

Material jetting is a likely AM technology for further composite fabrication, such as the work in [262] that produced dielectric ceramic and metal electrodes. This application is capable of producing high resolution microstructures using discrete nozzles to deposit different ink composition. However, due to the low deposition rate of the extrudate (300 nL/s), fabrication may take many hours to complete parts in the mesoscale. The control of material jetting colloidal ink feedstock allows for shear thinning to enable deposition of a cellular structure. Spanning gaps without contact between layers prevents electrical performance degradation while ensuring rigid deposition of the serpentine design, shown in Fig. 15.

The freeze-form extrusion fabrication (FEF) process for ceramic additive manufacturing has also been developed for graded compositions from alumina (Al_2O_3) to zirconia (ZrO_2) [184] and extended the application to FGMs from tungsten (W) to zirconium carbide (ZrC) [191]. The deposition of high solids loading ceramic pastes for the FEF process has many sensitivities, as shown in

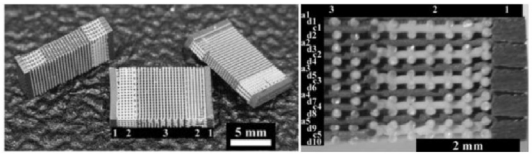

Fig. 15. (a) Application of Direct Writing to fabricate Ni-$BaTiO_3$ dielectrics (b) cross section of a specimen terminal [262].

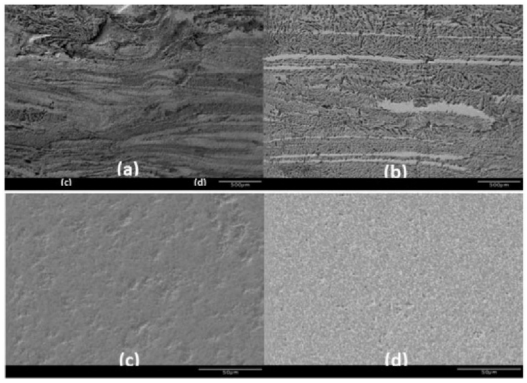

Fig. 16. SEM images of the cross-sectional microstructure of (a). 62.5%ZrC + 37.5%W, FEF fabricated, (b). 87.5%ZrC + 12.5%W, FEF fabricated, (c). 50%ZrC + 50%W, FEF fabricated; (d). 50%ZrC + 50%W, isostatic pressed [191].

Fig. 16a and b, which show striations due to improper mixing. The ZrC rich phase is the darker area, while the W rich phase is the lighter area. Defects such as porosity and heterogeneous distribution of phases in the FEF-FGM represent an area of continual study to improve mechanical properties of fabricated specimens. A 50/50 ratio of ZrC/W was fabricated using FEF which yielded a microstructure comparable to traditional pressing methods, Fig. 16c and d. However, mechanical properties of the FEF flexural samples are still considerably lower, averaging 73–31 MPa across the sample with increasing W content. This compares to the isostatic sample, averaging 224–404 MPa with increasing W content.

4. Materials issues in additive manufacturing

4.1. Binding mechanisms

AM processes are only possible through an efficient binding of additive layers. The binding technique determines the process speed and the part properties. The binding might be classified into 4 categories, as schematically shown in Fig. 17. They include i) secondary phase assisted binding, ii) chemically induced binding, iii) solid state sintering and iv) liquid fusion.

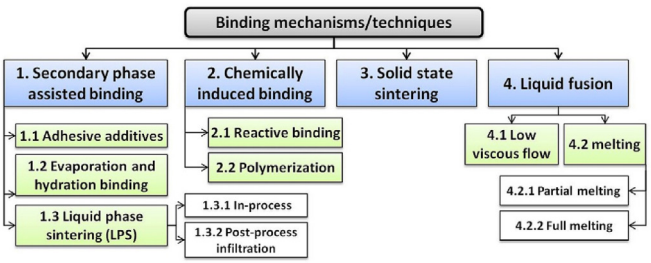

Fig. 17. Overview of binding mechanisms/techniques enabling AM processes.

4.1.1. Secondary phase assisted binding

Many AM processes (e.g., binder jetting, SLS, sheet lamination, etc.) use a secondary phase to bind the materials together. Secondary binding phases (in the forms of liquids, powders, coatings, etc.) can be added using different techniques such as mixing, coating, nozzle injection, etc. The binding is accomplished

through adhesive additives, evaporation and hydration binding, or liquid phase sintering (LPS).

4.1.1.1. Adhesive additives. During binder jetting, adhesive materials can be incorporated in the main material by embedding into the powder bed or addition through automated nozzles. The adhesive binder can be liquid or dry. A liquid binder (such as some polymer resins and inks in inkjet printing technology) contains all the binding components in the printed liquid. In comparison, dry adhesive can be added to the powder bed which binds the powder (physically or chemically) after interacting with the deposited liquid. Coatings of polyvinylpyrrolidone (a water-soluble polymer binder) on the powder particles chemically binds powders after being exposed to a solvent such as water [45,287,288]. Adhesive coatings are also commonly used in sheet lamination techniques where the sheet layers are bonded together after applying heat and/or pressure [314].

4.1.1.2. Evaporation-assisted and hydration-activated binding. A common concern with binder additives is the binder residue that may affect purity and properties of final parts. There are, however, volatile binders that can be evaporated after binding, leaving little or no residue. For example, chloroform can bind some biodegradable polyesters and then evaporate during the 3D printing process. The main drawback is the need for a post-processing treatment to improve the part strength [240,287]. Hydration-activated binding is another powder binder jetting technique that uses a simple liquid (e.g., water) to selectively bind the self-binding powder bed (such as plasters and cements). In this method, no adhesive is required since hydration is sufficient to activate the setting reactions.

4.1.1.3. Liquid phase sintering (LPS). This category applies to powder bed fusion AM processes that use a melt/liquid of a secondary phase to bind the primary matrix material (usually high melting point metals or ceramics). According to this mechanism, the secondary phase should have a low melting point and a good wettability with the higher melting point powder material (which remains solid during the process). This mechanism is applicable to material systems such as stainless steel bound by copper [174] (see Fig. 18), glass bound by PA12 [57,174], or WC bound by Co [176,179,207], but it may lead to porosity. Further densification is however possible through a post-process infiltration route (which is also a LPS mechanism), either by using a similar (e.g., infiltration of SiC-Si system with molten Si [217]—Fig. 19) or a dissimilar liquid melt material (such as infiltration of WC-Co system with a molten bronze [179,207]).

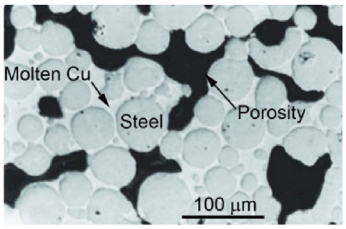

Fig. 18. Porous LPS stainless steel skeleton bound by Cu [173].

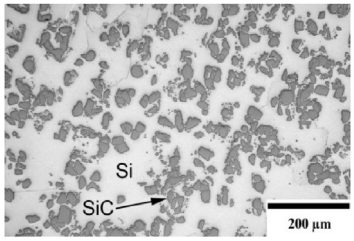

Fig. 19. LPS resulted dense microstructure of a SLS made part from Si-SiC after infiltration by Si [217].

4.1.2. Chemically induced binding

Some AM processes (such as vat photopolymerization processes, material jetting, etc.) use the chemical reactivity of material constituents to bind the layered material without the use of any secondary phases. This so-called chemically induced binding can be divided into reactive binding and polymerization.

4.1.2.1. Reactive binding. This mechanism involves the use of thermally activated chemical reactions between two types of powders or between powders and atmospheric gases to form a by-product which binds the powders together. Aluminum can react with the N_2 atmosphere used commonly in SLS machines, creating an AlN phase binding the Al particles [116,173,258].

4.1.2.2. Polymerization. Polymerization, discussed in Section 3.1.2, is crosslinking of a photo-curable resin, which hardens/sets the material. This process is also applicable to some ceramic powders suspended in a liquid resin [132,214,266].

4.1.3. Solid state sintering

Solid state sintering (SSS) is a solid diffusion binding mechanism. However, solid state sintering is mostly applied as a post-processing technique, e.g., furnace post-sintering to densify porous ceramics after removing/debinding the polymer binder.

4.1.4. Liquid fusion

Most AM processes (material extrusion, material jetting, directed energy deposition and powder bed fusion) use a liquid fusion binding mechanism. Liquid fusion is a rapid mass transport mechanism that may include low-viscosity flow in polymers and melting in metals.

4.1.4.1. Low-viscosity flow. This mechanism is commonplace in plastics where, via viscous flow, a heated plastic is fused to the previous layer upon deposition. Examples include heated thermoplastic filament or chocolate in material extrusion such as fused deposition modeling (FDM) and chocolate printing, wax material droplets deposited in materials jetting, or laser heated polymers in powder bed fusion processes such as SLS.

4.1.4.2. Melting. Melting (including partial melting and full melting) is another diffusion based mechanism that enables rapid fusion of metallic materials upon exposure to an intensive heat source such as a laser or electron beam. This mechanism can achieve completely dense metals from single materials. As a result, melting is the main AM approach to manufacture metal parts in directed energy deposition and powder bed fusion [173,174].

4.2. Defects in additive manufactured parts

4.2.1. Balling phenomenon

Balling was first reported for AM in 1992 [40] and is in fact a phenomenon that causes several physical defects such as porosity, micro-cracks or poor surface finish [197,285]. It occurs when the liquid material fails to wet the underlying substrate (due to the surface tension), spheroidizing the liquid due to Rayleigh Taylor

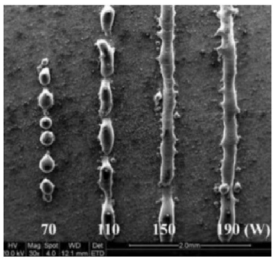

Fig. 20. Balling phenomenon at low laser power in SLM of 316L stainless steel. Shown is the top surface of the powder bed with a single vertical laser scan at indicated laser powers. Scan speed was 200 mm/s [197].

instability [58]. This results in a rough and bead-shaped scan track (e.g., in powder bed laser fusion processes), increasing the surface roughness and increasing the porosity, Fig. 20. Since contaminations can reduce the wetting degree, it is very important to prevent/minimize oxidation films and contamination [170,173].

4.2.2. Porosity

Porosity is a common defect in AM products since most of the binding mechanisms are driven by temperature changes, gravity and capillary forces without applying external pressure. As shown in Fig. 21, porosity can be found as irregular pores (e.g., due to shrinkage, lack of binding/fusion/melting, or material feed shortage, often occurring at the border of molten tracks) and spherical pores (commonly due to trapped gas, Marangoni turbulences in the melt region, material evaporation, etc., often occurring within the molten tracks).

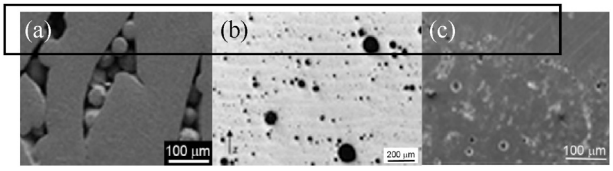

Fig. 21. Porosity from (a) lack of melting in EBM of Ti6Al4V [245], (b) gas in SLM of AlSi10Mg [310], and (c) lack of fusion and evaporation in SLS of a polymer elastomer (source KU Leuven).

4.2.3. Cracks

Cracking is a serious problem in AM materials forming due to several reasons. For example, laser based AM metal-based processes (laser cladding, SLM, etc.) are known to introduce large amounts of thermal stresses, originating from the rapid shrinkage of the melt pool and/or high temperature gradients in the solid material. Some examples of the cracks formed in AM materials are shown in Fig. 22. Obviously, materials with lower resistance to thermal shock (cf, ceramics [311] or brittle metals [302]) are more susceptible to crack formation. Compositional segregation and drying and shrinking of binder material are other factors that may give a rise to cracking [147,170,171,215,233].

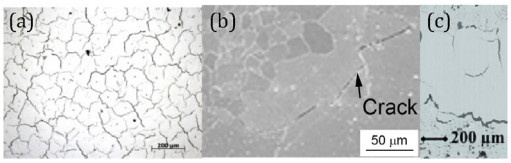

Fig. 22. Cracks in (a) SLM produced Hastelloy C276 metal superalloy [302], (b) alumina ceramic piece made by SLS/SLM without preheating [81], and (c) ethanol-alumina suspension infiltrated alumina produced by indirect SLS (cracks are formed within infiltrated regions) [82].

4.2.4. Distortion and delamination

Distortion/warpage/deflection is a defect that can originate from the stresses caused by changes in material volume (e.g., shrinkage of polymerization in stereolithography [152] or contraction of heated plastic filament extruded in FDM [305]) or large thermal gradients within parts [215]. In extreme cases, deflection may induce delamination, splitting the parts. This depends on the material characteristics, processing parameters and approaches [70]. Examples of distortion and delamination in SLM parts are shown in Fig. 23.

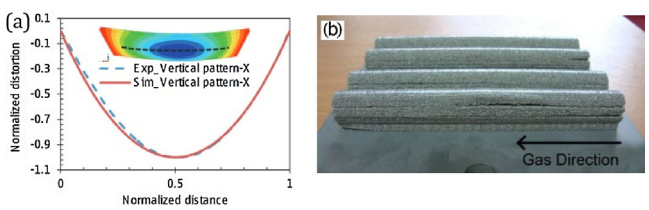

Fig. 23. (a) Experimental and simulation of distortion in a steel based SLM material [192] and (b) delamination in stainless steel SLM parts made along inert gas flow circulation (stimulating a larger thermal gradient) [68].

4.2.5. Poor surface finish

Poor surface finish is another concern in AM parts. It originates from different factors such as the 'staircase' effect associated with layer thickness and building orientation, coarse deposit beads (e.g., coarse filament in FDM or large extruded chocolate beads in chocolate printers), low tool precision (e.g., large electron beam heat affected field in EBM), surface tension and balling (as common in powder bed fusion methods), or semi-melted powders (e.g., powder and support material attached to down-facing surfaces in SLM). Poor surface finish can even be caused by aging of the used material, e.g., the extensively used polyamide powders in SLS may lead to poor surface quality appearing as an orange peel surface. Although surface roughness can be improved using a smaller deposit bead (or powder) and reduced layer thickness, this practice may reduce the production rate. Poor surface finish of complex AM components may necessitate post AM treatments such as grit blasting, mechanical grinding, laser polishing, chemical etching, etc., increasing the production cost [69,104,148,236,255,269].

4.2.6. Chemical degradation and oxidation

In many AM processes (especially those subjected to a high temperature), atmospheric conditions (such as oxygen content, humidity, etc.) must be strictly controlled. This is to prevent/minimize degradation and oxidation. Degradation/oxidation may lead to depolymerization in AM of polymers or result in oxide films/inclusions in AM of metals, harming the physical and mechanical properties. In addition to the atmospheric conditions, processing parameters such as higher energy input or working temperature can also increase chemical degradation and oxidation [92,173,317]. For example, higher laser energies in SLS of some polymers may lead to an unwanted smoking from degradation and depolymerization of the products (Fig. 24), reducing the mechanical properties [71].

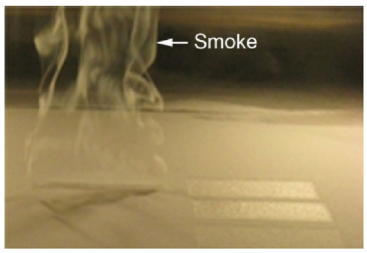

Fig. 24. Smoke during SLS of a polymer elastomer processed using a high energy input (Source: KU Leuven).

5. Properties of AM parts

5.1. Mechanical properties of AM parts

The nature of the interface between layers and, for powder-based AM processes, individual particles, affects mechanical properties. For example, in polymeric material extrusion, the deposited bead of material has good mechanical properties, but the interface between beads is compromised because the long-chain polymer molecules lie parallel to the interface rather than crossing it. The same is true for polymer laser sintering respecting both the layer interface and particle-to-particle interfaces. This is the reason that laser sintered polyamide has a maximum elongation of about 60% compared to injection molding where ductilities exceeding 300% are obtained [181].

The primary effect of porosity is to lower the stress at which fast fracture occurs. For ceramics, it widens the probability distribution

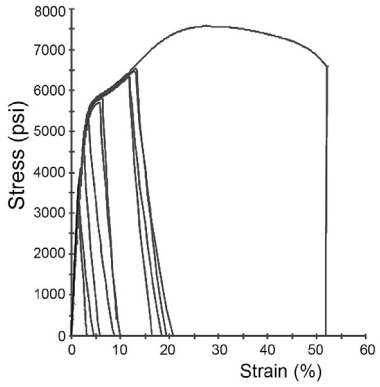

Fig. 25. Overlapping tension test results for laser sintered polyamide with varying amounts of engineered porosity [182].

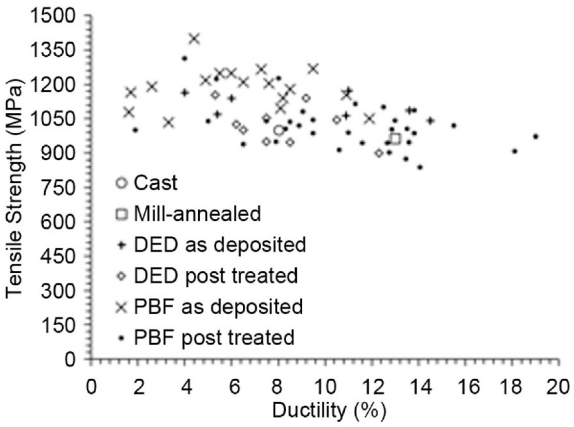

Fig. 26. Ultimate tensile strength versus ductility for Ti–6Al–4V fabricated by DED and PBF in as-deposited and heat treated conditions compared with data for cast and mill-annealed Ti–6Al–4V. The data show a general tradeoff between strength and ductility, and that heat treatment generally leads to reduction of strength and increase in ductility [34].

for fracture (i.e., decreases the Weibull modulus). Fig. 25 shows overlapping stress-strain curves for laser sintered polyamide samples with varying amounts of engineered porosity ranging between 0–40% [182]. Ductility and strength both increase as the porosity decreases. For high porosity samples, the fracture stress was below the yield strength and elongation measured as strain was also low. As the porosity was reduced, the strength increased significantly, approaching the yield strength. However, due to the steep slope of the elastic portion of the stress–strain curve, the strain to fracture remained low, less than 10%. For residual porosity in the 10–15% range, the fracture stress fell above the yield strength and below the tensile strength, resulting in a modest amount of measureable plasticity between 10–30%. When the porosity fell below about 5%, full ductility of 50–60% was restored.

In general, face-centered-cubic nonferrous metals (e.g., lead and copper) are most defect-tolerant, followed by ferrous and other nonferrous metals, polymers, elastomers, natural materials and finally ceramics. Mechanical properties have varying degrees of dependence on defect structures present. From most defect tolerant to least defect tolerant, in general, are stiffness, strength/hardness, ductility, fatigue and fracture.

Post-processing may be used to mitigate or eliminate defect structures in AM parts. Standard practice for safety-critical metal parts is to hot isostatic press (HIP) [25,26]. HIP may not be effective for elimination of interlayer defects depending on their nature. For example, oxide layers may not be affected by HIP. HIP has the capability effectively to eliminate porosity.

5.1.1. Strength

The yield and ultimate tensile strengths in additively manufactured metals are typically equal to, or greater than, the strength of their cast, wrought, or annealed counterparts (e.g., Refs. [34,127]). This is due to the rapid solidification of the melt pool during AM processing, which results in fine microstructural features, including fine grains, or closely-spaced dendrites.

Classical Hall–Petch grain size strengthening [129,238] describes the relationship between the yield strength of a material and the average grain diameter. With decreasing grain size, or fine microstructural features interrupting dislocation motion, the yield strength of a material increases. The fine microstructural features in metals made by AM impede dislocation motion, resulting in higher yield strengths than their conventionally processed and annealed counterparts.

Often, yield and ultimate tensile strengths in additively manufactured materials are not strongly anisotropic, with average strength values in the build (transverse) and longitudinal directions within statistical variation (e.g., Refs. [34,47,127,307]). However, when epitaxial growth of grains occurs during solidification (Fig. 7a), elongated grains may grow in the build direction, and the microstructure may be textured, or exhibit preferred crystallographic orientations. For example in Ti-6Al-4V, growth occurs along the [100] direction of the high temperature body-centered cubic beta-phase. However, upon cooling below the beta-transus of 980 °C, the prior-beta grains transform to hexagonal close-packed alpha laths. As there are 12 variants for this transformation, the resulting alpha-lath structure has been found to not be textured, and therefore, the texture itself does not impact mechanical properties [11,19,47,166,260].

When comparing ultimate tensile strengths in as-deposited Ti-6Al-4V made by DED and PFB, the strengths achieved by both methods, using a range of laser power and scanning speeds, are relatively similar as shown in Fig. 26.

These materials can be heat treated to homogenize the microstructure, or recrystallize and coarsen the grains, which results in a decrease in yield and ultimate tensile strengths, as shown in Fig. 26. Additionally, if the strength is limited by significant gas entrapment porosity or lack-of-fusion defects, HIP can be used to close and 'heal' the internal pores and defects in the samples, resulting in an increase in ductility [34].

The strength in polymeric materials made by AM may be impacted by defects, or insufficient interlayer adhesion and molecular bonding, which would result in higher strengths parallel to continuous laser passes or filament deposition lines and lower strengths perpendicular to these features. In a study on laser sintered polyamide 11, it was demonstrated that the tensile and yield strengths showed no direction dependence and were equivalent (within scatter) in the build direction and two in-plane directions as shown in Fig. 27.

Ceramics are intrinsically brittle due to the directional nature of the ionic and covalent bonding which prevents classical dislocation motion. Strength is generally assessed using three-or four-point bend testing [22,23] and is strongly dependent on defects whose size and shape are statistically variant. The strength of ceramics follows Weibull statistics [309]. High Weibull moduli are desirable, as this results in a narrow range of stress over which most parts will fail. Fig. 28 shows a Weibull plot for silicon nitride parts which were material extruded after compounding with a proprietary binder [61]. Some parts after binder burnout had large residual porosity with pore size exceeding 100 μm. The Weibull modulus for these specimens was 4.2. Removing the large pores through improvements to the process including redesigning the flow nozzle resulted in an increase in Weibull modulus to 15.1.

AM ceramics for which Weibull statistics have been applied include extrusion freeform fabrication of alumina [141] and alumino-silicates [202], fused deposition of ceramics silicon nitride [61], vat polymerization of silicon nitride [293], laminated object manufacturing of silicon carbide [163] and 3D printing of calcium phosphate [50] and alumina [234].

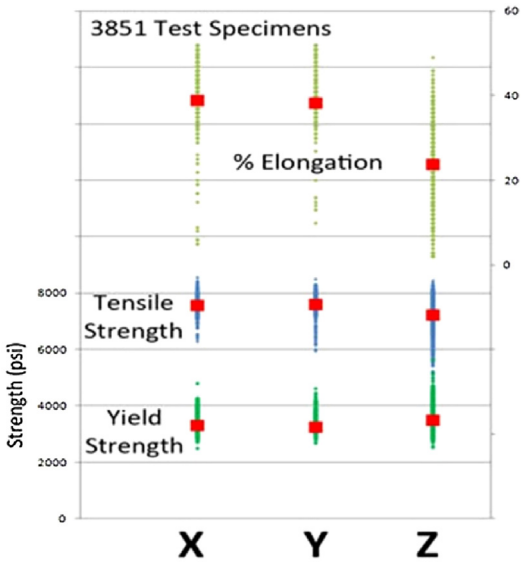

Fig. 27. Yield strength, ultimate tensile strength, and elongation in the build direction (Z), and two in-plane directions (X and Y) for laser sintered polyamide 11 (3851 tests, commercial builds). The data show that the yield and ultimate tensile strengths are largely unaffected by testing direction, whereas ductility in the Z direction is nearly 50% lower than in the X and Y direction [37].

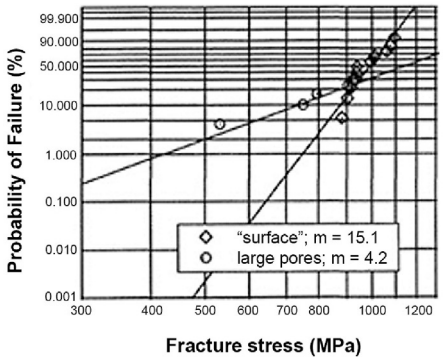

Fig. 28. Weibull statistics for material extruded silicon nitride after binder burnout. Specimens with large pores exhibited a low Weibull modulus [61].

5.1.2. Stiffness

The elastic modulus, or stiffness, of a material is decreased by porosity, as pores contribute no stiffness to the component. Empirical studies by Wachtman and MacKenzie [206] on the impact of pores on the elastic modulus E of porous ceramics have shown that the modulus decreases polynomially with respect to the modulus E_0 of the same fully dense ceramic. Thus, a major concern for ceramics in AM is the ability to produce monolithic components with little to no voids or cracks [346].

Additionally, work on cast steel by Bert [36] has been performed to describe the relationship between the elastic modulus and the shape and size of pores. Hardin et al. [133] described the elastic modulus of cast steel as:

$$\frac{E}{E_0} = \left(1 - \frac{p}{p_0}\right)^n$$

where n is an empirical exponent, and p_0 is the largest porosity at which a uniform porosity can exist in a representative volume element, and serves as a cutoff value that gives zero stiffness. Both n and p_0 depend on the size and shape of the microstructural pores, Fig. 29 [36].

While the elastic modulus in AM metals is not frequently reported, researchers have shown that with 97–99.7% relative density, the elastic modulus of Ti-6Al-4V made by PBF ranges from 80–94% of the 118 GPa modulus of bulk Ti-6Al-4V [291].

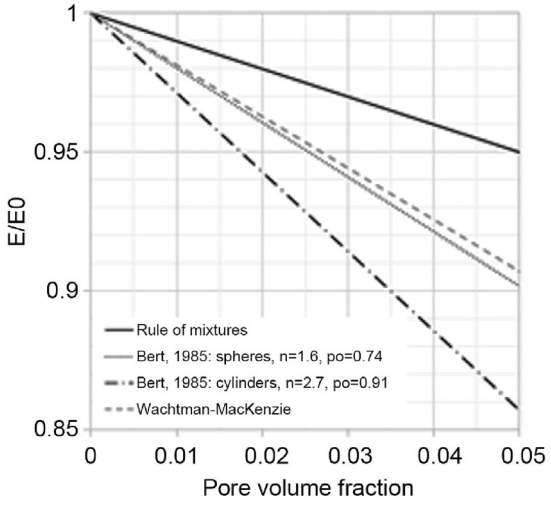

Fig. 29. Modulus of porous material normalized by modulus of fully dense material as a function of pore volume fraction [36,206].

5.1.3. Ductility

The ductility of materials made by AM is largely limited by internal defects, such as gas entrapment porosity (Fig. 21) or lack-of-fusion defects in metals (Fig. 30), insufficient interlayer adhesion in polymers, and cracks introduced during sintering of ceramic components.

Internal defects and surface roughness in as-deposited components provide discontinuous surfaces and therefore locations for stress concentrations under loading. These stress concentrations limit the far-field stress that can be applied to the material before it fails. In metallic materials, lack-of-fusion results in long sharp pores, which locally amplify the stress in components. In addition, the fine microstructural features due to rapid solidification lead to increased strength but reduced ductility due to limited dislocation motion, Fig. 26. This combination of internal defects and fine microstructure results in lower tensile failure strain in AM titanium and steel alloys compared to their wrought or annealed counterparts [12,18,47,76,88,90,96,103,122,124,137,139,140,153,167,187,205,222,246,296,301,307,322,329,336,338].

In addition, the epitaxial growth of grains in AM (Figs. 7 a and 31 a), resulting in elongated anisotropic grains, can result in limited ductility perpendicular to the build direction. For example, in Ti-6Al-4V made by DED, it was shown that grain-boundary alpha can be found decorating the prior-beta grain boundaries, resulting in a preferential crack path serving to separate grains when applying tension in the longitudinal direction, and therefore a reduced ductility, Fig. 31. Tension in the build (transverse) direction is not impacted negatively by the grain boundary phase [47].

In polymeric materials, insufficient molecular bonding between layers and inter-layer porosity results in delamination during loading in the build direction. Leigh et al., [182] showed that elongation to failure could be described in terms of porosity using an approach for sintered metals [134]:

$$\frac{\varepsilon_p}{\varepsilon_b} = \frac{(1-p)^{3/2}}{\sqrt{(1+Cp^2)}}$$

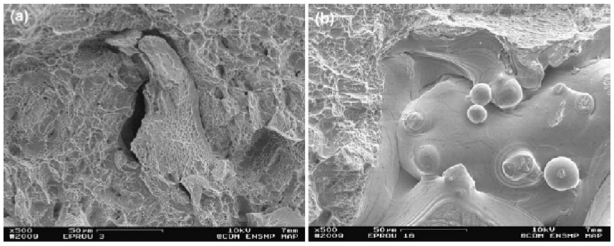

Fig. 30. Fracture surfaces of Ti–6Al–4V tensile samples made by PBF and tested in the (a) longitudinal direction, and (b) transverse (build) direction exposing lack-of-fusion defects [296].

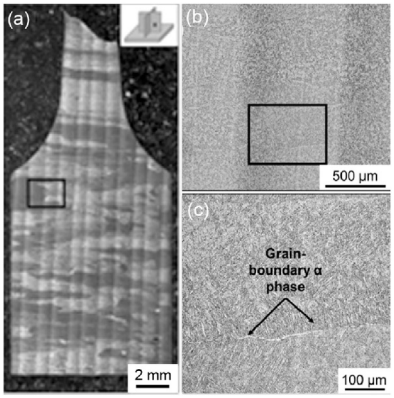

Fig. 31. Optical images of Ti–6Al–4V made by DED AM where the build direction is horizontal: (a) broken tensile sample where vertical lines correspond to subsequent layers and large prior beta grains grow in the build direction, (b) inset in (a), and (c) inset in (b) showing grain boundary alpha between prior beta grains [47].

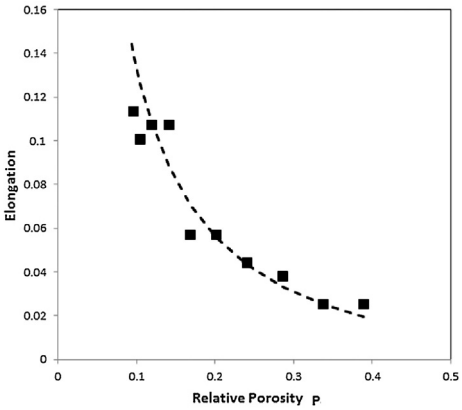

Fig. 32. Elongation versus relative porosity for laser sintered polyamide 12 [182].

where ε_p and ε_b are ductilities with porosity p and full density, respectively and C is a constant, as shown in Fig. 32.

5.1.4. Toughness

Fulcher et al. and Kempen et al. studied the impact toughness of two aluminum alloys made by PBF: AlSi10Mg and Al6061 [112,155]. Standard 10 mm square cross section specimens were tested. Fulcher et al. found that the impact toughness in AlSi10Mg was isotropic, with a value of 0.04 J/mm^2 in the longitudinal and transverse directions, which can be attributed to the relatively equiaxed grains characteristic of builds in this material. However, the impact energy was anisotropic in Al 6061, with an impact energy of 0.015 J/mm^2 in the horizontal direction (fracture along the build direction), and 0.07 J/mm^2 in the vertical direction (fracture along the layer direction). The micrographs of this material reveal a columnar grain growth along the build direction, which provides a preferential crack path along the build direction, resulting in significantly lower impact energy in that configuration [112]. The similar fracture surfaces in AlSi10Mg from the two orientations confirms that there is no change in fracture mechanism or path, while the fracture surfaces of Al 6061 show a stark difference between directions, as shown in Fig. 33.

Niino and Uehara studied the impact toughness of PEEK and polyamide produced using laser sintering [228]. They found that the Izod notched impact energy was 2.36 kJ/m^2 for laser sintered polyamide, compared to 9 kJ/m^2 for injection molded polyamide. As they also reported lower yield stresses in PEEK and polyamide made by laser sintering as compared with injection molded, it is postulated that insufficient bonding between layers during laser sintering resulted in weakened interfaces, and therefore lower strength and impact resistance in these materials.

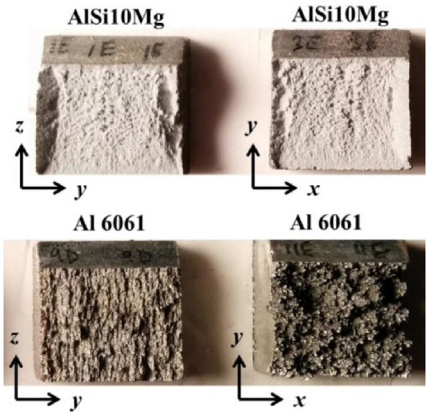

Fig. 33. Fracture surfaces of Al-alloy Charpy specimens made by PBF AM, showing the lack of direction-dependent fracture surfaces in AlSi10Mg contrasted with fracture surfaces in Al 6061 that are strongly direction-dependent [112].

5.1.5. Fatigue

Rapid solidification from the melt in AM results in residual stress buildup due to shrinkage as the molten pool becomes solid as well as additional thermal contraction during cooling. Both lead to significant buildup of residual stresses in components made by AM (e.g., Ref. [86]). In addition to resulting in warpage of components, these residual stresses can drive crack nucleation and growth in components.

A review on fatigue comparing stress-fatigue life curves for conventionally processed and additively manufactured Ti-6Al-4V is given in Ref. [196]. A summary plot is shown in Fig. 34. This review revealed the following general trends:

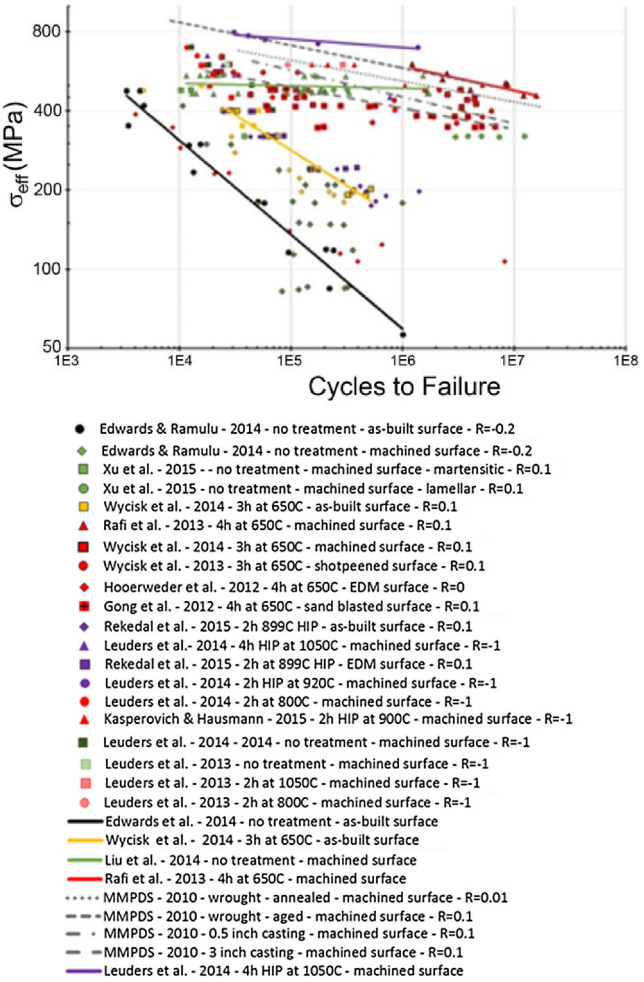

Fig. 34. Fatigue-life curves for Ti–6Al–4V made by laser PBF with and without heat treatment and surface machining for R ~ 0 and R = −1 [196]. R equals the ratio of the minimum stress to the maximum stress during cyclic loading.

- The rough surfaces in as-deposited AM samples provided stress concentrations, resulting in accelerated crack nucleation and growth, and reduced fatigue performance compared to machined versions of the same samples
- Heat treatment without pressure relieved residual stresses and improved fatigue life
- Heat treatment with pressure closed pores and improved fatigue life

Leuders and co-workers highlighted the importance of residual stress and microstructural morphology on the fatigue properties of Ti-6Al-4V made by PBF [187]. They performed fatigue crack growth testing on Ti-6Al-4V made by PBF AM with and without heat treatment at 800 °C and 1050 °C, and hot isostatic pressing (HIP) at 920 °C and 1000 bar. They showed that the as-deposited samples, which contained residual stresses, had lower ΔK_{th} required for crack growth, compared to heat treated and HIP samples. They postulated that pores in the samples had a less significant impact on ΔK_{th}, or crack growth, than the residual stresses, as all heat treated and HIP samples had similar ΔK_{th}. However, they showed that pores and microstructural morphology have a significant impact on the high cycle fatigue performance, or the crack initiation.

Limited work has been performed to assess the fatigue performance in polymers made by AM. Ziemian et al. studied the fatigue behavior of ABS made by FDM AM, specifically investigating the dependence of fatigue properties on hatch orientation as well as sample orientation [344]. They showed that for unidirectional samples, the fatigue life was shortest when applying tension perpendicular to the deposition direction, and longest when applying tension along the direction of the road paths. A higher fatigue life was achieved with samples fabricated using +45°/−45° hatch pattern with respect to the tensile loading direction. This points to the importance of delamination between deposits as well as the alignment of polymer chains along the deposition direction, resulting in the most resistance to failure along the deposition direction, and the least when serving to separate deposits.

Moore and Williams studied the fatigue performance of the rubber-like TangoBlackPlus, as well as the interface between this rubbery material and the stiffer VeroWhitePlus in the Object Polyjet 3D printing system [219]. They showed that the interface between the two disparate materials had more scatter in terms of fatigue life, but not a lower fatigue life than the monolithic TangoBlackPlus itself.

5.2. Optical properties

The predominance of additive manufacturing (AM) literature dealing with optical properties centers on transparency. Vat polymerization has for some time had commercial transparent materials available. Material jetting technologies also have various commercial grades of transparent materials. Other processes such as Rapid freeze prototyping are naturally amenable to production of transparent parts in ice [337]. A DED approach has been developed by which transparent quartz parts were produced using a filament side-feed mechanism into a laser power source [204]. The issue with other AM technologies including ink-jet printing, laser sintering and fused deposition modeling, is avoiding internal reflections from surfaces which impede transparency.

Niino at the University of Tokyo was among the first to explore use of refractive index matched infiltrants to produce transparent laser sintered parts, Fig. 35 [229,230]. Suwanprateeb and Suwanpreuk produced transparent ink-jet printed parts by mixing polymethyl methacrylate (PMMA) powders with maltodextrin binders followed by infiltration with a heat-curing acrylic [271]. It showed the maximum transmittance (25–30%) was achieved at binder with 10% PMMA. Binder elimination prior to infiltration was an essential step in increasing the transmittance, without which the sample transmittance only increased 1%. This is related to the decrease in porosity from infiltration and a generation of strong interfacial bonding between PMMA particles and the acrylate infiltrant material.

Fig. 35. CastformTM polystyrene as-laser sintered (left, n = 1.588) and after infiltration with index-of-refraction (n) matching ultraviolet curing epoxy (n = 1.582), right [229].

Ahn et al. [7] analyzed two post-processing techniques to increase the optical transmittance of the part made of ABSi by fused deposition modeling (FDM). ABSi is Stratasys' medical grade thermoplastic ABS. The effect of raised temperature and infiltration of resin in post-processing were studied. The best elevation temperature was 180 °C where transmittance increased by 10%. Resin infiltration followed by surface sanding was the optimal post processing; transmittance increased by 16%.

Optically translucent parts made using vat polymerization have been used in the biomedical field to produce 3D biodegradeable scaffolds for bone ingrowth [64] and to develop biomodels for cranioplasty [67]. Suwanprateeb and Suwanpreuk [271] fabricated DSM 11120 resin sheet using SL system RS 3500 as a comparison to a specimen made using PMMA with binder jetting. They found SL parts had 20% higher transmittance and 1000 MPa lower flexural modulus compared to the PMMA part.

Optically translucent parts termed lithophanes rely on the optical properties of the feedstock for service performance [332–335]. A lithophane, illustrated in Fig. 36, is a typically flat representation of an image designed to be backlit and based on varying the part thickness to generate variations in grayscale. The physical basis for varying grayscale with local part thickness is described by absorption of visible light as it passes through a solid medium (Beer–Lambert Equation, cf., [332]).

Lithophanes have been successfully created using laser sintered polyamide 12 [332–335], stereolithographic white resin Proto-GenTM O-XT 18420, [334] and material-extrusion polylactic acid. Stereolithography produces higher resolution images than laser sintering or material extrusion, but due to a low absorption constant for the stereolithography resin investigated, the lithophane contrast was not as good as that for laser sintered polyamide.

For laser sintered polyamide, the maximum lithophane thickness is about 5 mm, based on the absorption characteristics of the polymer. For parts built in the XY plane [144], the local part thickness is defined by the number of layers. At a standard 100 μm layer thickness, the total number of layers is at most approximately 50 layers, which results in only 50 levels of grayscale. Parts built vertically in the XZ plane have significantly better quality, although the build time is lengthened by an order of magnitude or more

Fig. 36. Front-lit and backlit images of a polyamide 12 lithophane created using laser sintering. The part is 10.2 cm wide, 14.5 cm tall with maximum thickness of 0.5 cm. The Z direction is vertical [335].

[335]. The lithophane backlit image quality was improved for laser sintered polyamide by the following factors: build orientation on edge, 5 mm maximum lithophane thickness, monochromatic 540 nm light (green), absorption constant α equal to approximately 0.5 mm^{-1} [335].

5.3. Electrical properties

The electrical properties of materials are affected by the manufacturing process, since this impacts the final microstructure of the material. Microstructural effects on electrical properties are associated with the mobility of a conducting species, generally electrons. For AM polymers, interest in electrical properties is generally either to maintain the intrinsic electrical insulating characteristic or to use additives to increase electrical conductivity. To a first approximation, AM ceramic and metal parts exhibit electrical behavior similar to traditional manufacturing methods so long as the effect of residual porosity is managed. The porosity effect may be approximated using a conventional empirical formula [114].

Polymer insulating characteristics are measured in terms of the dielectric strength or dielectric constant. Using ASTM D3755 [24], the dielectric strength of LS polyamide 12 has been measured to be 30 kV/mm which is consistent with the injection molded value [284]. The dielectric strength drops to 7 kV/mm for high-speed sintering due to the introduction of carbon particles designed to couple to the heat source during manufacturing. The dielectric constant decreased with increasing AC frequency. At 100 Hz, LS polyamide 12 had a dielectric constant of 2.5, compared to 3.5 for high-speed sintering and 3-4 for injection molded material [284]. The electrical dissipation factor was constant between 10–1000 Hz and was measured to be 0.025 (LS), 0.04 (high-speed sintering) and 0.03–0.08 (injection molding). The dielectric constants and loss factors have been measured for material jetting [94]. The dielectric constant for three photopolymers (Vero White, Tango Black, Shore 95) was approximately 3. The loss tangent for Vero White was measured to be 0.0285 at 1.5 GHz. Peterkin et al., have studied the dielectric strength of stereolithography parts [239].

Improvements to AM polymer electrical conductivity are accomplished by additions of conductive media, typically carbon. Additions of 4% nanosized carbon black to polyamide 12 increased the electrical conductivity from 4×10^{-10} S/cm to 10^{-4} S/cm [27]. Similar results were obtained when 5% carbon multiwalled nanotubes were mixed in polyamide 11 [178], for which electrical conductivity improved from 10^{-11} to 10^{-4} S/cm by altering the mixing and distribution of the nanotubes within the polymer.

The electrical conductivity of LS graphite with a transient phenolic binder was improved by increasing the post-processing polymer burn-out temperature from near 0 S/cm (600 °C) to 250 S/cm (1300 °C) [10]. A LS natural graphite sample had 400 S/cm [274]. In both studies, additions of carbon fibers reduced the electrical conductivity, which was consistent with the lower intrinsic conductivity of the fibers (300 S/cm) compared to graphite (1000 S/cm) [39].

LiO_2–ZrO_2–SiO_2–Al_2O_3 (LZSA) has been tape cast and sheet laminated using Laminated Object Manufacturing. The dielectric constant was 8.6 with a loss tangent equal to 0.004 [118].

Additive manufacturing has been used for production of both metal [16,17] and plastic [20] based electrodes for electric discharge machining (EDM). Laser melting was used to produce a TiB_2-CuNi composite with 25% porosity and electrical conductivity of 1.938 S/cm [17]. EDM electrodes were also produced in 63Mo-37(90Cu-10Ni) premixed powder by laser melting [16]. EDM results showed that the Mo composite removes material twice as fast as solid copper electrodes and with only 10% of the tool wear.

6. Future outlook for materials in additive manufacturing

Future developments are set to facilitate the progression of AM technologies toward competing favorably with established production technologies but also allowing new design freedoms as a function of materials supply. This is also set to complement the geometric capabilities of AM.

6.1. Enhanced material performance

Enhancing materials performance and suitability for AM processes will remain a key research area. Reliability, traceability and the specific development of materials which have comparable properties to 'bulk' equivalents but are optimized to AM processes have formed the basis of significant levels of research.

For example, aluminum alloys require significant materials redesign to be processed effectively. Efforts have been made to understand these facets following Abe et al.'s exploration of the problem [1]. Louvis et al. [203] performed fundamental analysis of an AlSi12Mg alloy and 6061. Poor metallurgy is often compounded with morphological defects associated with powder bed processes which are shown clearly to be characteristic of process as well as material and are as such not random [8,275].

Early adopters of metal based AM have been high value markets, as the associated cost is currently relatively high. Poor machinability of these materials creates an opportunity for AM processes [87]. For example, Acharya and Das have demonstrated that microstructural control is possible in Nickel based alloys during laser based repair methods for worn gas turbine components [5]. This presents an interesting avenue for researchers in this area who seek to maintain control of the microstructure throughout original part manufacture.

Jackson et al. in their exploration of design methodologies for AM highlight the opportunity and difficulties associated with adapting both process and design methodology for the creation of functionally graded structures in AM [145]. While visionary in some respects, the manufacturing tools and associate materials development to achieve this have been limited. The merits of this approach through conventional manufacturing techniques are explored in Mortensen and Suresh's review [220] on powder processes for functional grading. Through manual control of materials, Abioye et al. [2] have demonstrated that NiTi graduated alloys can be created in single DMD processes with controlled microstructures. This presents an interesting opportunity for designers seeking to apply location-specific functionality in a single part. Similarly Syed et al. [273] delivered both wire and powder to build functionally graded coatings.

6.2. AM material property databases

There is value in assembling property information for AM into a database form. This enables designers to specify AM processes and materials efficiently. Graphical representation of salient properties such as shown in Fig. 37 provides a means for facile comparison of

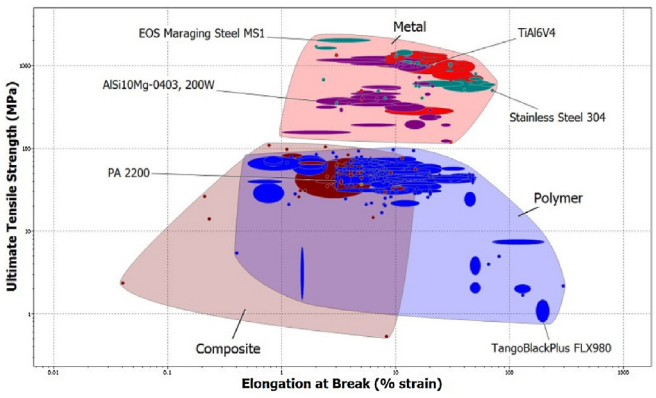

Fig. 37. Summary plot of part ultimate tensile strength versus elongation for AM materials. The plot is based on property data for additive manufacturing materials from the Senvol Database™ using the CES Selector™ [120]. Image courtesy of Granta Design Ltd (Cambridge, UK).

processes and materials. Plots of this type graphically illustrate the relative application space for different classes of materials. NIST is initiating an open source materials database for AM.

6.3. Novel feedstock

Beyond the free form structural design capability permitted to manufacturers through the use of AM for metals, is the ability to alloy in process through the supply of elemental powders [63]. This then creates significant flexibility in the composition of a component. Gu et al. [127] highlighted contributions in this respect across Fe, Cu and intermetallic materials systems and in doing so demonstrates the breadth of capability this approach provides. This is an excellent review of this area to date.

Traditional feedstocks for SLM, EBM and DMD techniques are drawn from pre-alloyed powders. Here, powder morphology and composition is tightly controlled by the supplier to meet the powder specification required for process compatibility. However, the in-situ alloying of variable composition feedstocks allows new opportunities in materials design. Through enthalpic homogenization [257] composition can be controlled to a degree. Although further work is clearly required to manage this in process, the capability will be of clear interest to industrial users. The formation of several systems through adapted feedstocks has been demonstrated including Ti-6Al-4V [326], Ti-6Al-4V/WC [105] and Ti/TiAl [113]. However, this approach is easily translated across materials systems for entirely new, batch-wise production of materials much more efficiently compared to foundry-scale production.

The formulation of materials specifically for AM continues to be an important area in the progression of metal-based systems. Poor weldability, characterised by a number of factors including high-viscosity melt pools or cracking on solidification, limits the process-ability of some material systems. This has been explored by Vora et al. [298] for aluminum alloys in particular. These alloys have limited usage in SLM currently as alloys with high Si and Mg content are required. Attempts to overcome this have involved the addition of Si to 7XXX [218] series aluminum feedstocks to enhance material behavior in processes with noted success. Another approach involves mixing elemental powders which process in AM more successfully than prealloyed powder followed by a post-processing homogenization anneal. This has been shown in the 6xxx Al system [252]. There are several additional systems which are prime for similar investigation including nickel superalloys where the poor weldability of these limits their process-ability in AM methods.

6.4. AM manufacturability index

Based on progress in materials for AM, the field is matured to a point where it is feasible to consider a new manufacturing index for AM akin to those associated with conventional manufacturing, e.g., weldability, castability, formability. This “additive manufacturability index” or “AMability” would be a measure of the overall success with which a material may be processed by additive manufacturing. The index would clearly be process specific, based on Table 1. In this regard, the AM index would share with casting and welding indices which likewise are process specific. Considerations might include the ease with which proper feedstock is formed, processability in the AM fabricator, resulting microstructure and associated properties, surface finish/ease of finishing, geometric accuracy and post-processing requirements. Researchers and commercial interests have identified materials that are reasonably processable by AM, including polyamide and Ti-6Al-4V for powder bed fusion, PLA and ABS for material extrusion, epoxies for vat polymerization, etc. They have identified parameters important for screening feedstocks as well. Assignment of a qualitative or semi-quantitative index would, like the other manufacturing indices, provide designers and developers with a useful tool for selecting materials for specific applications, particularly when a choice must be made between AM and conventional processing for a specific material.

By way of example, Verbelen has proposed a semi-quantitative manufacturing index for laser sintering of polymers [294]. Included in the considerations are melt flow (zero-shear viscosity, melt temperature, coalescence behavior), powder morphology, powder formation and flow, crystallization (difference of melting temperature and crystallization temperature, shrinkage) and recyclability/powder degradation. Using weighting functions on specific parameters, he obtained a summary index. Table 2 lists his results for a few polymers.

Table 2
Additive manufacturability indices for laser sintered polymers [294].

Polymer	Additive manufacturability index
Polyamide 11	8.4
Polyamide 12	8.3
Thermoplastic polyurethane	7.4
PEEK	6.4
Polyethylene	6.4
Polystyrene	8.7

7. Summary and conclusions

Materials play a dominant role in additive manufacturing (AM), particularly when considering materials for engineered structural applications. To be successful, materials must be formed into proper feedstock, have appropriate characteristics for processing in the specific AM fabricator, and must have acceptable service properties. AM fabricators are currently formed into seven groups: binder jetting, directed energy deposition, material extrusion, material jetting, powder bed fusion, sheet lamination, and vat polymerization. Specific materials particularly amenable to AM processing are listed by each category. Coverage of polymers (amorphous and semicrystalline thermoplastics, and thermosets), metals, ceramics and composites is provided. Binding mechanisms in AM are reviewed. Service properties of AM materials are surveyed, including strength, stiffness, ductility, toughness, fatigue, optical properties and electrical properties.

Attention is currently focused on understanding the origin of defects in AM parts and eliminating them. These include porosity, binding defects, interfaces and microstructural effects. The authors propose the development of a process-specific additive manufacturing index to guide materials selection for AM.

Acknowledgments

The authors are grateful to the following individuals who assisted in writing and reviewing the manuscript: S. Dadbakhsh (KU Leuven), B. Vrancken (KU Leuven), and T. Starr (University of Louisville).

References

[1] Abe F, Osakada K, Shiomi M, Uematsu K, Matsumoto M (2001) The Manufacturing of Hard Tools from Metallic Powders by Selective Laser Melting. *Journal of Materials Processing Technology* 111(1–3):210–213.
[2] Abioye TE, Farayibi PK, Kinnel P, Clare AT (2015) Functionally Graded Ni–Ti Microstructures Synthesised in Process by Direct Laser Metal Deposition. *International Journal of Advanced Manufacturing Technology* 79(5):843–850.
[3] Abioye TE, Farayibi PK, McCartney DG, Clare AT (2016) Effect of Carbide Dissolution on the Corrosion Performance of Tungsten Carbide Reinforced Inconel 625 Wire Laser Coating. *Journal of Materials Processing Technology* 231:89–99.
[4] Abioye TE, Folkes J, Clare AT, McCartney DG (2013) Concurrent Inconel 625 Wire and WC Powder Laser Cladding: Process Stability and Microstructural Characterization. *Journal of Surface Engineering* 29(9):647–653.
[5] Acharya R, Das S (2015) Additive Manufacturing of IN100 Superalloy Through Scanning Laser Epitaxy for Turbine Engine Hot-Section Component Repair:

Process Development, Modeling, Microstructural Characterization, and Process Control. *Metallurgical and Materials Transactions A* 46(9):3864–3875.
[6] Agarwala MK, van Weeren R, Yaidyanathan R, Bandyopadhyay A, Carrasquilo G, Jamalabad V, Langrana N, Safari A, Garofalini S, Danforth SC, Burlew J, Donaldson R, Whalen P, Ballard C (1995) Structural Ceramics by Fused Deposition of Ceramics. *Proceedings of SFF Symposium*, Austin TX USA, 1–8.
[7] Ahn S, Lee CS, Felong W (2004) Development of Translucent FDM Parts by Post-Processing. *Rapid Prototyping Journal* 10(4):218–224.
[8] Ahuja B, Karg M, Nagulin K, Schmidt M (2014) Laser Beam Melting of High Strength Aluminium Alloys EN AW-6061 and EN AW-6082. in Drstvensek o, (Ed.) *Proceedings of 5th International Conference on Additive Technologies*, 153–158.
[9] Ainsley C, Reis N, Derby B (2002) Freeform Fabrication by Controlled Droplet Deposition of Powder Filled Melts. *Journal of Materials Science* 37:3155–3161.
[10] Alayavalli K, Bourell DL (2010) Fabrication of Modified Graphite Bipolar Plates by Indirect Selective Laser Sintering (SLS) for Direct Methanol Fuel Cells. *Rapid Prototyping Journal* 16(4):268–274.
[11] Al-Bermani SS, Blackmore ML, Zhang W, Todd I (2010) The Origin of Microstructural Diversity, Texture, and Mechanical Properties in Electron Beam Melted Ti–6Al–4V. *Metallurgical and Materials Transactions A* 41(13):3422–3434.
[12] Alcisto J, Enriquez A, Garcia H, Hinkson S, Steelman T, Silverman E, Valdovino P, Gigerenzer H, Foyos J, Ogren J, Dorey J, Karg K, McDonald T, Es-Said OS (2011) Tensile Properties and Microstructures of Laser-Formed Ti–6Al–4V. *Journal of Materials Engineering and Performance* 20#2:203–212.
[13] Amado Becker AF (2016) *Characterization and Prediction of SLS Processability of Polymer Powders with Respect to Powder Flow and Part Warpage. (Doctoral thesis)*, ETH Zürich, Switzerland.
[14] Amado A, Schmid M, Levy G, Wegener K (2011) Advances in SLS Powder Characterization. *Solid Freeform Fabrication Symposium*, Austin, TX, 438–452.
[15] Amato KN, Gaytan SM, Murr LE, Martinez E, Shindo PW, Hernandez J, Collins S, Medina F (2012) Microstructures and Mechanical Behavior of Inconel 718 Fabricated by Selective Laser Melting. *Acta Materialia* 60:2229–2239.
[16] Amorim FL, Lohrengel A, Neubert V, Higa CF, Czelusniak T (2014) Selective Laser Sintering Of MoCuNi Composite to Be Used as EDM Electrode. *Rapid Prototyping Journal* 20(1):59–68.
[17] Amorim FL, Lohrengel A, Schaefer G, Czelusniak T (2013) A Study on The SLS Manufacturing and Experimenting of TiB_2-CuNi EDM Electrodes. *Rapid Prototyping Journal* 19(6):418–442.
[18] Amsterdam E, Kool GA (2009) High Cycle Fatigue of Laser Beam Deposited Ti–6Al–4V and Inconel 718. *25th International Committee on Aeronautical Fatigue Symposium, Springer Amsterdam*, The Netherlands, 1261–1274.
[19] Antonysamy AA, Meyer J, Prangnell PB (2013) Effect of Build Geometry on the β-Grain Structure and Texture in Additive Manufacture of Ti6Al4V by Selective Electron Beam Melting. *Materials Characterization* 84:153–168.
[20] Arthur A, Dickens PM, Cobb RC (1996) Using Rapid Prototyping to Produce Electrical Discharge Machining Electrodes. *Rapid Prototyping Journal* 2(1):4–12.
[21] Ashby MF (2011) Designing Hybrid Materials. *Acta Materialia* 51(19):5801–5821.
[22] ASTM C1161-13 (2013) *Standard Test Method for Flexural Strength of Advanced Ceramics at Ambient Temperature*, ASTM, International, West Conshohocken, PA.
[23] ASTM C1239-13 (2013) *Standard Practice for Reporting Uniaxial Strength Data and Estimating Weibull Distribution Parameters for Advanced Ceramics*, ASTM, International, West Conshohocken, PA.
[24] ASTM D3755-86 (1986, Reapproved 1995) Standard Test Method for Dielectric Breakdown Voltage and Dielectric Strength of Solid Electrical Insulating Materials under Dielectric Strength of Solid Electrical Insulating Materials under Direct-Voltage Stress. ASTM International, West Conshohocken, PA.
[25] ASTM F2924-14 (2014) *Standard Specification for Additive Manufacturing Titanium-6 Aluminum-4 Vanadium with Powder Bed Fusion*, ASTM, International, West Conshohocken, PA.
[26] ASTM F3001-14 (2014) *Standard Specification for Additive Manufacturing Titanium-6 Aluminum-4 Vanadium ELI (Extra Low Interstitial) with Powder Bed Fusion*, ASTM, International, West Conshohocken, PA.
[27] Athreya SR, Kalaitzidou K, Das S (2010) Processing and Characterization of a Carbon Black-Filled Electrically Conductive Nylon-12 Nanocomposite Produced by Selective Laser Sintering. *Materials Science and Engineering A* 527(10–11):2637–2642.
[28] Augsburg M, Storch S, Nissen F, Will G (2004) Rapid Prototyping with Ceramic Filled Epoxy Resin by Optoforming. *Rapid Prototyping Journal* 10(4):225–231.
[29] Balla VK, Bose S, Bandyopadhyay A (2008) Processing of Bulk Alumina Using Laser Engineered Net Shaping. *International Journal of Applied Ceramic Technology* 5(3):234–242.
[30] Bartolo P, Kruth J-P, Silva J, Levy G, Malshe M, Rajurkar K, Mitsuishi M, Ciurana J, Leu M (2012) Biomedical Production of Implants by Additive Electro-Chemical and Physical Processes. *CIRP Annals Manufacturing Technology* 61(2):635–655.
[31] Bass LB, Meisel NA, Williams CB (2015) Exploring Variability in Material Properties of Multi-material Jetting Parts. *Proceedings of SFF Symposium*, Austin TX USA, 993–1006.
[32] Bassi GL (1993) Formulation of UV-Curable Coatings—How to Design Specific Properties. in Fouassier JP, Rabek JF, (Eds.) *Radiation Curing in Polymer Science and Technology—Vol II: Photoinitiated Systems*, Elsevier Applied Science, London & New York239.
[33] Baumers M, Tuck C, Hague R (2015) Selective Heat Sintering versus Laser Sintering: Comparison of Deposition Rate, Process Energy Consumption and Cost Performance. *Proceedings of SFF Symposium*, Austin TX USA, 109–121.
[34] Beese AM, Carroll BE (2015) Review of Mechanical Properties of Ti–6Al–4V Made by Laser- Based Additive Manufacturing Using Powder Feedstock. *JOM* 68#3:724–734.
[35] Bergström D (2008) *The Absorption of Laser Light by Rough Metal Surfaces (Doctoral-Thesis)*, Luleå University of Technology, Sweden.
[36] Bert CW (1985) Prediction of Elastic Moduli of Solids with Oriented Porosity. *Journal of Materials Science* 20:2220–2224.
[37] Bourell D (2012) The Evolution of Materials for Additive Manufacturing. *4th International Conference on Additive Technologies*, Maribor, Slovenia10 pages.
[38] Bourell DL (2016) Perspectives on Additive Manufacturing. *Annual Review of Materials Research* 46:1–18.
[39] Bourell DL, Leu MC, Chakravarthy K, Guo N, Alayavalli K (2011) Graphite-Based Indirect Laser Sintered Fuel Cell Bipolar Plates Containing Carbon Fiber Additions. *CIRP Annals-Manufacturing Technology* 60(1):275–278.
[40] Bourell D, Marcus H, Barlow JW, Beaman JJ (1992) Selective Laser Sintering of Metals and Ceramics. *International Journal of Powder Metallurgy* 28#4:369–381.
[41] Brandl E, Baufeld B, Leyens C, Gault R (2010) Additive Manufactured Ti–6Al–4V Using Welding Wire: Comparison of Laser and Arc Beam Deposition and Evaluation with Respect to Aerospace Material Specifications. *Physics Procedia* 5B:595–606.
[42] Brandl E, Heckenberger U, Holzinger V, Buchbinder D (2012) Additive Manufactured AlSi10Mg Samples Using Selective Laser Melting (SLM): Microstructure, High Cycle Fatigue, and Fracture Behavior. *Materials & Design* 34:159–169.
[43] Buchbinder D, Meiners W, Pirch N, Wissenbach K, Schrage J (2014) Investigation on Reducing Distortion by Preheating During Manufacture of Aluminum Components Using Selective Laser Melting. *Journal of Laser Applications* 26:012004.
[44] Buchbinder D, Schleifenbaum H, Heidrich S, Meiners W, Bültmann J (2011) High Power Selective Laser Melting (HP SLM) of Aluminum Parts. *Physics Procedia* 12A:271–278.
[45] Calvert P (2001) Inkjet Printing for Materials and Devices. *Chemistry of Materials* 13:3299–3305.
[46] Carroll BE, Otis RA, Borgonia JP, Suh JO, Dillon RP, Shapiro AA, Hofmann DC, Liu ZK, Beese AM (2016) Functionally Graded Material of 304L Stainless Steel and Inconel 625 Fabricated by Directed Energy Deposition: Characterization and Thermodynamic Modeling. *Acta Materialia* 108:46–54.
[47] Carroll BE, Palmer TA, Beese AM (2015) Anisotropic Tensile Behavior of Ti–6Al–4V Components Fabricated with Directed Energy Deposition Additive Manufacturing. *Acta Materialia* 87:309–320.
[48] Carter LN, Attallah MM, Reed RC (2012) Laser Powder Bed Fabrication of Nickel-Base Superalloys: Influence of Parameters; Characterisation, Quantification and Mitigation of Cracking. *Superalloys 2012*, John Wiley & Sons, Inc., Hoboken, NJ577–586.
[49] Casalino G, Campanelli SL, Contuzzi N, Ludovico AD (2015) Experimental Investigation and Statistical Optimisation of the Selective Laser Melting Process of a Maraging Steel. *Optics & Laser Technology* 65:151–158.
[50] Castilho M, Gouveia B, Pires I, Rodrigues J, Pereira M (2015) The Role of Shell/core Saturation Level on the Accuracy and Mechanical Characteristics of Porous Calcium Phosphate Models Produced By 3Dprinting. *Rapid Prototyping Journal* 21(1):43–55.
[51] Cesarano III J. (1999) A Review of Robocasting Technology. *Solid Freeform and Additive Fabrication: A Materials Research Society Symposium*, Boston MA, 133–139.
[52] Cesarano III J, Baer TA, Calvert JP (1997) Recent Developments in Freeform Fabrication of Dense Ceramics from Slurry Deposition. *Proceedings of SFF Symposium*, Austin TX USA, 25–33.
[53] Cesarano J, King BH, Denham HB (1998) Recent Developments in Robocasting of Ceramics and Multimaterial Deposition. *Proceedings of SFF Symposium*, Austin TX USA, 697–704.
[54] Cesarano J, Segalman R, Calvert P (1998) Robocasting Provides Mould-Less Fabrication from Slurry Deposition. *Ceramic Industry* 148:94–101.
[55] Chapman GM, Akehurst EE, Wright WB (1971) Cocoa Butter and Confectionery Fats: Studies Using Programmed Temperature X-ray Diffraction and Differential Scanning Calorimetry. *Journal of the American Oil Chemists' Society* 48(12):824–830.
[56] Cheng B, Chou K (2014) Thermal Stresses Associated with Part Overhang Geometry in Electron Beam Additive Manufacturing: Process Parameter Effects. *Proceedings of SFF Symposium*, Austin TX USA, 1076–1087.
[57] Childs THC, Tontowi AE (2001) Selective Laser Sintering of a Crystalline and a Glass-Filled Crystalline Polymer: Experiments and Simulations. *Proceedings of the Institution of Mechanical Engineers Part B: Journal of Engineering Manufacture* 215:1481–1495.
[58] Chivel A (2014) Ablation Phenomena and Instabilities under Laser Melting of Powder Layers. *8th International Conference on Photonic Technologies LANE*, Erlangen, Germany7 pages.
[59] Chung H, Das S (2006) Processing and Properties of Glass Bead Particulate-Filled Functionally Graded Nylon-11 Composites Produced by Selective Laser Sintering. *Materials Science and Engineering A* 437(2):226–234.
[60] Chung H, Das S (2008) Functionally Graded Nylon-11/Silica Nanocomposites Produced by Selective Laser Sintering. *Materials Science and Engineering A* 487(1–2):251–257.
[61] Clancy R, Jamalabad V, Whalen P, Bhargava P, Dai C, Rangarajan S, Wu S, Danforth S, Langrana N, Safari A (1997) Fused Deposition of Ceramics: Progress towards a Robust and Controlled Process for Commercialization. *Proceedings of SFF Symposium*, Austin TX USA, 185–194.
[62] Clare AT, Chalker PR, Davies S, Sutcliffe CJ, Tsopanos S (2008) Selective Laser Sintering of Barium Titanate–Polymer Composite Films. *Journal of Materials Science* 43:3197–3202.
[63] Clayton RM (2013) *The Use of Elemental Powder Mixes in Laser-Based Additive Manufacturing, (MS Thesis)*, Missouri University of Science and Technology.
[64] Cook MN, Fisher JP, Dean D, Rimna C, Mikos AG (2002) Use of Stereolithography to Manufacture Critical-Sized 3D Biodegradable Scaffolds for Bone

Ingrowth. *Journal of Biomedical Materials Research Part B:Applied Biomaterials* 64B(2):65–69.
[65] Crivello JV, Dietliker K. (1998) Photoinitiators for Free Radical, Cationic & Anionic Photopolymerisation. in Bradley G, (Ed.) *Chemistry & Technology of UV & EB Formulation for Coatings Inks & Paints*, 2nd ed., Vol. IIIJohn Wiley & Sons, Inc., Chichester & New Yorkin association with SITA Technology Ltd., London, UK.
[66] Crivello JV, Lee JL, Conlon DA (1983) Photoinitiated Cationic Polymerization with Multifunctional Vinyl Ether Monomers. *Journal of Radiative Curing* 10 (1):6–13.
[67] D'Urso PS, Effeney DJ, Earwaker WJ, Barker TM, Redmond MJ, Thompson RG, Tomlinson FH (2000) Custom Cranioplasty Using Stereolithography and Acrylic. *British Journal of Plastic Surgery* 53(3):200–204.
[68] Dadbakhsh S (2012) *Mechanical Engineering: The Selective Laser Melting of Metals and In-Situ Aluminium Matrix Composites (Doctoral Thesis)*, University of Exeter, Exeter, UKhttp://hdl.handle.net/10036/3840.
[69] Dadbakhsh S, Hao L, Kong CY (2010) Surface Finish Improvement of LMD Samples Using Laser Polishing. *Virtual and Physical Prototyping* 5:215–221.
[70] Dadbakhsh S, Hao L, Sewell N (2012) Effect of Selective Laser Melting Layout on the Quality of Stainless Steel Parts. *Rapid Prototyping Journal* 18:241–249.
[71] Dadbakhsh S, Verbelen L, Vandeputte T, Strobbe D, Van Puyvelde P, Kruth J-P (2016) Effect of Powder Size and Shape on the SLS Processability and Mechanical Properties of a TPU Elastomer. *Physics Procedia* 83:971–980.
[72] Dadbakhsh S, Vrancken B, Kruth J-P, Luyten J, Van Humbeeck J (2016) Texture and Anisotropy in Selective Laser Melting of NiTi Alloy. *Materials Science and Engineering: A* 650:225–232.
[73] Das M, Balla VK, Basu D, Bose S, Bandyopadhyay A (2010) Laser Processing of SiC-Particle-Reinforced Coating on Titanium. *Scripta Materialia* 63(4):438–441.
[74] Das M, Bysakh S, Basu D, Sampath Kumar TS, Balla VK, Bose S, Bandyopadhyay A (2011) Microstructure, Mechanical and Wear Properties of Laser Processed SiC Particle Reinforced Coatings on Titanium. *Surface and Coatings Technology* 205(19):4366–4373.
[75] De Hazan Y, Heinecke J, Weber A, Graule T (2009) High Solids Loading Ceramic Colloidal Dispersions in UV Curable Media via Comb-Polyelectrolyte Surfactants. *Journal of Colloid and Interface Science* 337(1):66–74.
[76] De Lima MSF, Sankaré S (2014) Microstructure and Mechanical Behavior of Laser Additive Manufactured AISI 316 Stainless Steel Stringers. *Materials & Design* 55:526–532.
[77] de Obaldia EE, Jeong C, Grunenfelder LK, Kisailus D, Zavattieri P (2015) Analysis of the Mechanical Response of Biomimetic Materials with Highly Oriented Microstructures Through 3D Printing, Mechanical Testing and Modeling. *Journal of the Mechanical Behavior of Biomedical Materials* 48:70–85.
[78] Decker C, Decker D (1994) Kinetic and Mechanistic Study of The UV-Curing of Vinyl Ether Based Systems. *RadTech '94–North America UV/EB Conference and Exposition Conference Proceedings*, Orlando, Florida, USA, 602.
[79] Decker C, Viet TNT, Decker D, Weber-Koehl E (2001) UV-Radiation Curing of Acrylate/Epoxide Systems. *Polymer* 42:5531–5541.
[80] Decker C, Xuan HL, Viet TNT (1996) Photocrosslinking of Functionalized Rubber. III. Polymerization of Multifunctional Monomers in Epoxidized Liquid Natural Rubber. *Journal of Polymer Science Part A: Polymer Chemistry* 34:1771–1781.
[81] Deckers J (2013) *Selective Laser Sintering and Melting as Additive Manufacturing Methods to Produce Alumina Parts (Doctoral Thesis)*, KU Leuven, Leuven Belgium.
[82] Deckers J, Kruth J-P, Cardon L, Shahzad K, Vleugels J (2013) Densification and Geometrical Assessments of Alumina Parts Produced Through Indirect Selective Laser Sintering of Alumina–Polystyrene Composite Powder. *Strojniski Vestnik/Journal of Mechanical Engineering* 59:646–661.
[83] Deckers J, Shahzad K, Vleugels J, Kruth J-P (2012) Isostatic Pressing Assisted Indirect Selective Laser Sintering of Alumina Components. *Rapid Prototyping Journal* 18(5):409–419.
[84] Deckers J, Vleugels J, Kruth J-P (2014) Additive Manufacturing of Ceramics: A Review. *Journal of Ceramic Science and Technology* 5(4):245–260.
[85] Dehoff RR, Kirka MM, Sames WJ, Bilheux H, Tremsin AS, Lowe LE, Babu SS (2015) Site Specific Control of Crystallographic Grain Orientation Through Electron Beam Additive Manufacturing. *Materials Science and Technology* 31:931–938.
[86] Denlinger ER, Heigel JC, Michaleris P (2015) Residual Stress and Distortion Modeling of Electron Beam Direct Manufacturing Ti–6Al–4V. *Proceedings of the Institution of Mechanical Engineers Part B: Journal of Engineering Manufacture* 229(10):1803–1813.
[87] Diltemiz SF, Zhang S (2012) Superalloys for Super Jobs. *Aerospace Materials Handbook*, CRC Press, Boca Raton FL1–76.
[88] Dinda GP, Song L, Mazumder J (2008) Fabrication of Ti–6Al–4V Scaffolds by Direct Metal Deposition. *Metallurgical and Materials Transactions A* 39#12:2914–2922.
[89] Ding D, Pan Z, Cuiuri D, Li H (2015) Wire-Feed Additive Manufacturing of Metal Components: Technologies, Developments and Future Interests. *International Journal of Advanced Manufacturing Technology* 81:465–481.
[90] Donachie MJ (2000) *Titanium: A Technical Guide*, 2nd ed. ASM International, Materials Park, OH.
[91] Donachie MJ, Donachie SJ (2002) *Superalloys: A Technical Guide*, 2nd ed. ASM, International, Materials Park, OH.
[92] Drummer D, Wudy K, Drexler M (2014) Influence of Energy Input on Degradation Behavior of Plastic Components Manufactured by Selective Laser Melting. *Physics Procedia* 56:176–183.
[93] Du Y, Liu H, Shuang J, Wang J, Ma J, Zhang S (2015) Microsphere-Based Selective Laser Sintering for Building Macroporous Bone Scaffolds with Controlled Microstructure and Excellent Biocompatibility. *Colloids and Surfaces B Biointerfaces* 135:81–89.
[94] Dumene RL, Kennedy P, Williams CB, Sweeney D, Earle G (2015) Creating Embedded Radiofrequency Structures Using Polyjet Material Jetting. *Proceedings of SFF Symposium*, Austin TX USA, 1769–1787.
[95] Duro-Royo J, Mogas-Soldevila L, Oxman N (2015) Flow-Based Fabrication: an Integrated Computational Workflow for Digital Design and Additive Manufacturing of Multifunctional Heterogeneously Structured Objects. *Computer-Aided Design* 69:143–154.
[96] Edwards P, O'Conner A, Ramulu M (2013) Electron Beam Additive Manufacturing of Titanium Components: Properties and Performance. *Journal of Manufacturing Science and Engineering* 135#6:061016.
[97] Edwards P, Ramulu M (2014) Fatigue Performance Evaluation of Selective Laser Melted Ti–6Al–4V. *Materials Science and Engineering: A* 598: 327–337.
[98] Elomaa L, Kokkari A, Närhi T, Seppälä JV (2013) Porous 3D Modeled Scaffolds of Bioactive Glass and Photocrosslinkable Poly(ε-Caprolactone) by Stereolithography. *Composites Science and Technology* 74:99–106.
[99] Espalin D, Alberto Ramirez J, Medina F, Wicker R (2014) Multi-Material, Multi-Technology FDM: Exploring Build Process Variations. *Rapid Prototyping Journal* 20(3):236–244.
[100] Evans RS (2005) *Indirect Rapid Manufacturing of Silicon Carbide Composites (Doctoral Thesis)*, The University of Texas, Austin TX USA.
[101] Evans RS, Bourell DL, Beaman JJ, Campbell MI (2003) Reaction Bonded Silicon Carbide: SFF, Process Refinement and Applications. *Proceedings of SFF Symposium*, Austin TX USA, 414-422.
[102] Evans RS, Bourell DL, Beaman JJ, Campbell MI (2005) Rapid Manufacturing of Silicon Carbide Composites. *Rapid Prototyping Journal* 11(1):37–40.
[103] Facchini L, Magalini E, Robotti P, Molinari A, Höges S, Wissenbach K (2010) Ductility of a Ti–6Al–4V Alloy Produced by Selective Laser Melting of Prealloyed Powders. *Rapid Prototyping Journal* 16#6:450–459.
[104] Farayibi PK, Abioye TE, Murray JW, Kinnell PK, Clare AT (2014) Surface Improvement of Laser Clad Ti–6Al–4V Using Plain Waterjet and Pulsed Electron Beam Irradiation. *Journal of Materials Processing Technology* 218:1–11.
[105] Farayibi P, Clare A, Folkes J, McCartney D, Abioye T (2012) Laser Deposition of Ti–6Al–4V Wire with Varying WC Composition for Functionally Graded Components. *Proceedings of the 37th International MATADOR Conference*, vol. 10. 343–348.
[106] Farayibi PK, Folkes JA, Clare AT (2013) Laser Deposition of Ti–6Al–4V Wire with WC Powder for Functionally Graded Components. *Materials and Manufacturing Processes* 28(5):514–518.
[107] Farayibi PK, Folkes J, Clare A, Oyelola O (2011) Cladding of Pre-Blended Ti–6Al–4V and WC Powder for Wear Resistant Applications. *Surface and Coatings Technology* 206(2–3):372–377.
[108] Ferraris E, Vleugels J, Guo Y, Bourell D, Kruth J-P, Lauwers B (2016) Shaping of Engineering Ceramics by Electro, Chemical and Physical Processes. *CIRP Annals* 65(2):761–784.
[109] Fielding GA, Bandyopadhyay A, Bose S (2012) Effects of Silica and Zinc Oxide Doping on Mechanical and Biological Properties of 3D Printed Tricalcium Phosphate Tissue Engineering Scaffolds. *Dental Materials* 28(2):113–122.
[110] Fong, JW (2013) Photocurable resin composition for producing three dimensional articles having high clarity, US Patent 8,377,623.
[111] Fu Z, Schlier L, Travitzky N, Greil P (2013) Three-Dimensional Printing of SiSiC Lattice Truss Structures. *Materials Science and Engineering A* 560:851–856.
[112] Fulcher BA, Leigh DK, Watt TJ (2014) Comparison of AlSi10Mg and Al 6061 Processed Through DMLS. *Proceedings of the SFF Symposium*, Austin TX USA, 404–419.
[113] Gasper AND, Catchpole-Smith S, Clare AT (2017) In-Situ Synthesis of Titanium Aluminides by Direct Metal Deposition. *Journal of Materials Processing Technology* 239:230–239.
[114] German RM (2005) *Powder Metallurgy and Particulate Materials Processing*, Metal Powder Industries Federation, Princeton NJ389.
[115] Ghazanfari A, Li W, Leu MC, Hilmas GE (2016) A Novel Extrusion-Based Additive Manufacturing Process for Ceramic Parts. *Proceedings of the SFF Symposium*, Austin, TX, 1509–1529.
[116] Gibson I, Rosen D, Stucker B (2015) *Additive Manufacturing Technologies*, Springer, New York. (Chapters 4, 5 and 19).
[117] Gill TJ, Hon KKB (2004) Experimental Investigation into the Selective Laser Sintering of Silicon Carbide Polyamide Composites. *Proceedings of the Institution of Mechanical Engineers* 218(Part B 9).
[118] Gomes C, Travitzky N, Greil P, Acchar W, Birol H, Novaes de Oliveira AP, Hotza D (2011) Laminated Object Manufacturing of LZSA Glass-Ceramics. *Rapid Prototyping Journal* 17(6):424–428.
[119] Goodridge RD, Shofner ML, Hague RJM, McClelland M, Schlea MR, Johnson RB, Tuck CJ (2011) Processing of a Polyamide-12/Carbon Nanofibre Composite by Laser Sintering. *Polymer Testing* 30(1):94–100.
[120] Granta Design Limited (2016) Granta and Senvol Team up on Selection of Additive Manufacturing Processes and Materials, https://www.grantadesign.com/news/2016/senvol.shtml, Cambridge, United Kingdom.
[121] Griffin E, Mumm DR, Marshall DB (1996) Rapid Prototyping of Functional Ceramic Composites. *American Ceramic Society Bulletin* 75(7):65–68.
[122] Griffith ML, Ensz MT, Puskar JD, Robino CV, Brooks JA, Philliber JA, Smugeresky JE, Hofmeister WH (2000) Understanding the Microstructure and Properties of Components Fabricated by Laser Engineered Net Shaping (LENS). *MRS Proceedings* 625.
[123] Griffith ML, Halloran JW (1996) Freeform Fabrication of Ceramics via Stereolithography. *Journal of the American Ceramic Society* 79(10):2601–2608.
[124] Griffith ML, Keicher DM, Atwood CL, Romero JA, Smugeresky E, Harwell LD, Greene DL, Smugeresky JE, Harwell LD, Greene DL (1996) Free Form Fabrication of Metallic Components Using Laser Engineered Net Shaping (LENS™). *Proceedings of SFF Symposium*, Austin TX USA, 125–132.

[125] Gu D, Shen Y (2006) WC—Co Particulate Reinforcing Cu Matrix Composites Produced by Direct Laser Sintering. *Materials Letters* 60(29–30):3664–3668.
[126] Gu D, Shen Y (2008) Direct Laser Sintered WC-10Co/Cu Nanocomposites. *Applied Surface Science* 254(13):3971–3978.
[127] Gu DD, Meiners W, Wissenbach K, Poprawe R (2012) Laser Additive Manufacturing of Metallic Components: Materials, Processes and Mechanisms. *International Materials Reviews* 57#3:133–164.
[128] Hagedorn Y-C, Balachandran N, Meiners W, Wissembach K, Poprawe R (2011) SLM of Net-Shaped High Strength Ceramics: New Opportunities for Producing Dental Restorations. *Proceedings of the SFF Symposium*, Austin TX USA, 536–546.
[129] Hall EO (1951) The Deformation and Ageing of Mild Steel: III Discussion of Results. *Proceedings of the Physical Society Section B* 64:747–753.
[130] Halloran JW (1999) Freeform Fabrication of Ceramics. *British Ceramic Transactions* 98(6):299–303.
[131] Halloran JW, Griffith M, Chu T-M (2000) Stereolithography resin for rapid prototyping of ceramics and metals, US Patent #6,117,612.
[132] Halloran JW, Tomeckova V, Gentry S, Das S, Cilino P, Yuan D, Guo R, Rudraraju A, Shao P, Wu T, Alabi TR, Baker W, Legdzina D, Wolski D, Zimbeck WR, Long D (2011) Photopolymerization of Powder Suspensions for Shaping Ceramics. *Journal of the European Ceramic Society* 31:2613–2619.
[133] Hardin RA, Beckermann C (2007) Effect of Porosity on the Stiffness of Cast Steel. *Metallurgical and Materials Transactions A* 38A#12:2992–3006.
[134] Haynes R (1977) A Study of the Effect of Porosity Content on the Ductility of Sintered Metals. *Powder Metallurgy* 20(1):17–20.
[135] Hinczewski C, Corbel S, Chartier T (1998) Stereolithography for the Fabrication of Ceramic Three-dimensional Parts. *Rapid Prototyping Journal* 4(3):104–111.
[136] Hofmann DC, Kolodziejska J, Roberts S, Otis R, Dillon RP, Suh J-O, Liu Z-K, Borgonia J-P (2014) Compositionally Graded Metals: A New Frontier of Additive Manufacturing. *Journal of Materials Research* 29(17):1899–1910.
[137] Hollander DA, Von Walter M, Wirtz T, Sellei R, Schmidt-Rohlfing B, Paar O, Erli HJ (2006) Structural, Mechanical and in Vitro Characterization of Individually Structured Ti–6Al–4V Produced by Direct Laser Forming. *Biomaterials* 27#7:955–963.
[138] Hopkinson N, Erasenthiran P (2004) High s Peed Sintering— Early Research into a New Rapid Manufacturing Process. *Proceedings of the SFF Symposium*, Austin TX USA, 312–320.
[139] Hrabe N, Quinn T (2013) Effects of Processing on Microstructure and Mechanical Properties of a Titanium Alloy (Ti–6Al–4V) Fabricated Using Electron Beam Melting (EBM), Part 1: Distance from Build Plate and Part Size. *Materials Science and Engineering: A* 573:264–270.
[140] Hrabe N, Quinn T (2013) Effects of Processing on Microstructure and Mechanical Properties of a Titanium Alloy (Ti–6Al–4V) Fabricated Using Electron Beam Melting (EBM), Part 2: Energy Input, Orientation, and Location. *Materials Science and Engineering: A* 573:271–277.
[141] Huang T, Mason MS, Zhao X, Hilmas GE, Leu MC (2009) Aqueous-based Freeze-form Extrusion Fabrication of Alumina Components. *Rapid Prototyping Journal* 15(2):88–95.
[142] Idaszek J, Bruinink A, SĘwie?szkowski W (2015) Ternary Composite Scaffolds with Tailorable Degradation Rate and Highly Improved Colonization by Human Bone Marrow Stromal Cells. *Journal of Biomedical Materials Research Part A* 103(7):2394–2404.
[143] ISO/ASTM Standard 52900 (2015) *Standard Terminology for Additive Manufacturing – General Principles – Part 1: Terminology*, ASTM, West Conshohocken, PA.
[144] ISO/ASTM Standard 52921-13 (2013) *Standard Terminology for Additive Manufacturing-coordinate Systems and Test Methodologies*, ASTM, West Conshohocken, PA.
[145] Jackson TR, Liu H, Patrikalakis NM, Sachs EM, Cima MJ (1999) Modeling and Designing Functionally Graded Material Components for Fabrication with Local Composition Control. *Materials & Design* 20(2–3):63–75.
[146] Jacobs PF (1996) *Stereolithography and Other RP&M Technologies*, Society of Manufacturing Engineers, Dearborn, MI.
[147] James DM-C (2015) Additive Manufacturing of Components from Engineering Ceramics. *Additive Manufacturing*, CRC Press, Boca Raton FL311–330.
[148] Jamshidinia M, Kovacevic R (2015) The Influence of Heat Accumulation on the Surface Roughness in Powder-bed Additive Manufacturing. *Surface Topography: Metrology and Properties* 3:014003.
[149] Janaki Ram GD, Robinson C, Yang Y, Stucker BE (2007) Use of Ultrasonic Consolidation for Fabrication of Multi-material Structures. *Rapid Prototyping Journal* 13(4):226s–235s.
[150] Kaminski D (2011) *LASER MARKING: How to Choose the Best Laser for Your Marking Application*, Laser Focus World, http://www.laserfocusworld.com/articles/2011/04/laser-marking-how-to-choose-the-best-laser-for-your-marking-application.html.
[151] Kanagarajah P, Brenne F, Niendorf T, Maier HJ (2013) Inconel 939 Processed by Selective Laser Melting: Effect of Microstructure and Temperature on the Mechanical Properties under Static and Cyclic Loading. *Materials Science and Engineering: A* 588:188–195.
[152] Karalekas D, Aggelopoulos A (2003) Study of Shrinkage Strains in a Stereolithography Cured Acrylic Photopolymer Resin. *Journal of Materials Processing Technology* 136:146–150.
[153] Keicher DM, Miller WD (1998) LENS™ Moves Beyond RP to Direct Fabrication. *Metal Powder Report* 53#12:26–28.
[154] Kelly SM, Kampe SL (2004) Microstructural Evolution in Laser-deposited Multilayer Ti–6Al–4V Builds: Part I. Microstructural Characterization. *Metallurgical and Materials Transactions A* 35:1861–1867.
[155] Kempen K, Thijs L, Van Humbeeck J, Kruth J-P (2012) mechanical Properties of AlSi10Mg Produced by Selective Laser Melting. *Physics Procedia* 39:439–446.
[156] Kempen K, Thijs L, Van Humbeeck J, Kruth J-P (2015) Processing AlSi10Mg by Selective Laser Melting: Parameter Optimisation and Material Characterization. *Materials Science and Technology* 31:917–923.
[157] Kempen K, Vrancken B, Buls S, Thijs L, Van Humbeeck J, Kruth J-P (2014) Selective Laser Melting of Crack-free High Density M2 High Speed Steel Parts by Baseplate Preheating. *Journal of Manufacturing Science and Engineering* 136:061026-1–061026-6.
[158] Kempen K, Yasa E, Thijs L, Kruth J-P, Van Humbeeck J (2011) Microstructure and Mechanical Properties of Selective Laser Melted 18Ni-300 Steel. *Physics Procedia* 12A:255–263.
[159] Khan M, Dickens P (2012) Selective Laser Melting (SLM) of Gold (Au). *Rapid Prototyping Journal* 18:81–94.
[160] Kieback B, Neubrand A, Riedel H (2003) Processing Techniques for Functionally Graded Materials. *Materials Science and Engineeering A* 362(1–2):81–105.
[161] Kim J, Creasy TS (2004) Selective Laser Sintering Characteristics of Nylon 6/clay-reinforced Nanocomposite. *Polymer Testing* 23(6):629–636.
[162] King W, Anderson AT, Ferencz RM, Hodge NE, Kamath C, Khairallah SA (2015) Overview of Modelling and Simulation of Metal Powder Bed Fusion Process at Lawrence Livermore National Laboratory. *Materials Science and Technology* 31:957–968.
[163] Klosterman D, Chartoff R, Osborne N, Graves G (1997) Automated Fabrication of Monolithic and Ceramic Matrix Composites via Laminated Object Manufacturing (LOM). *Proceedings of SFF Symposium*, Austin TX USA, 537–550.
[164] Klosterman D, Chartoff R, Osborne N, Graves G (1997) Laminated Object Manufacturing, a New Process for the Direct Manufacture of Monolithic Ceramics and Continuous Fiber CMCs. *Proceedings of the 21st Annual Conference on Composites Ceramics Materials and Structures-8* 112–120.
[165] Klosterman D, Chartoff R, Osborne N, Graves G, Lightman A, Han G, Bezeredi A, Rodrigues S (1999) Development o F a Curved Layer LOM Process for Monolithic Ceramics and Ceramic Matrix Composites. *Rapid Prototyping Journal* 5(2):61–71.
[166] Kobryn PA, Semiatin SL (2003) Microstructure and Texture Evolution During Solidification Processing of Ti–6Al–4V. *Journal of Materials Processing Technology* 135#2–3:330–339.
[167] Koike M, Greer P, Owen K, Lilly G, Murr LE, Gaytan SM, Martinez E, Okabe T (2011) Evaluation of Titanium Alloys Fabricated Using Rapid Prototyping Technologies-electron Beam Melting and Laser Beam Melting. *Materials (Basel)* 4#10:1776–1792.
[168] Kou S (2003) *Welding Metallurgy*, 2nd ed. John Wiley & Sons, Hoboken NJ.
[169] Kruth JP (1991) Material Incress Manufacturing by Rapid Prototyping Techniques. *CIRP Annals Manufacturing Technology* 40(2):603–614.
[170] Kruth J-P, Dadbakhsh S, Vrancken B, Kempen K, Vleugels J, Humbeeck JV (2015) Additive Manufacturing of Metals via Selective Laser Melting: Process Aspects and Material Developments. *Additive Manufacturing*, CRC Press, Boca Raton FL69–99.
[171] Kruth J-P, Froyen L, Van Vaerenbergh J, Mercelis P, Rombouts M, Lauwers B (2004) Selective Laser Melting of Iron-based Powder. *Journal of Materials Processing Technology* 149:616–622.
[172] Kruth J-P, Leu MC, Nakagawa T (1998) Progress in Additive Manufacturing and Rapid Prototyping. *CIRP Annals Manufacturing Technology* 47(2):525–540.
[173] Kruth J-P, Levy G, Klocke F, Childs THC (2007) Consolidation Phenomena in Laser and Powder-bed Based Layered Manufacturing. *CIRP Annals Manufacturing Technology* 56(2):730–759.
[174] Kruth J-P, Mercelis P, Vaerenbergh JV, Froyen L, Rombouts M (2005) Binding Mechanisms in Selective Laser Sintering and Selective Laser Melting. *Rapid Prototyping Journal* 11:26–36.
[175] Kumar S, Kruth J-P (2010) Composites by Rapid Prototyping Technology. *Materials & Design* 31(2):850–856.
[176] Kumar S, Kruth J-P, Froyen L (2008) Wear Behaviour of SLS WC-Co Composites. *Proceedings of SFF Symposium*, Austin TX USA, 543–557.
[177] Kunze K, Etter T, Grässlin J, Shklover V (2015) Texture, Anisotropy in Microstructure and Mechanical Properties of IN738LC Alloy Processed by Selective Laser Melting (SLM). *Materials Science and Engineering: A* 620:213–222.
[178] Lao SC, Kan MF, Lam CK, Chen DZ, Koo JH, Moon T, Londa M, Takatsuka T, Kuramoto E, Wissler G, Pilato L, Luo ZP (2010) Polyamide 11-carbon Nanotubes Nanocomposites: Processing, Morphological, and Property Characterization. *Proceedings of SFF Symposium*, Austin TX USA, 451–467.
[179] Laoui T, Froyen L, Kruth J-P (1999) Effect of Mechanical Alloying on Selective Laser Sintering of WC-9Co Powder. *Powder Metallurgy* 42:203–205.
[180] Ledesma-Fernandez J, Tuck C, Hague R (2015) High Viscosity Jetting of Conductive and Dielectric Pastes for Printed Electronics. *Proceedings of SFF Symposium*, Austin TX USA, 40–55.
[181] Leigh DK (2012) A Comparison of Polyamide 11 Mechanical Properties Between Laser Sintering and Traditional Molding. *Proceedings of the SFF Symposium*, Austin TX USA, 574–605.
[182] Leigh DK, Bourell DL, Beaman JJ (2011) Effect of In-plane Voiding on the Fracture Behavior of Laser Sintered Polyamide. *Proceedings of the SFF Symposium*, Austin TX USA, 453–463.
[183] Leong CC, Lu L, Fuh JYH, Wong YS (2002) In-situ Formation of Copper Matrix Composites by Laser Sintering. *Materials Science and Engineering A* A338(1–2):81–88.
[184] Leu MC, Deuser BK, Tang L, Landers RG, Hilmas GE, Watts JL (2012) Freeze-form Extrusion Fabrication of Functionally Graded Materials. *CIRP Annals-Manufacturing Technology* 61:223–226.
[185] Leu MC, Garcia DA (2014) Freeze-form Extrusion Fabrication of Ceramic Part with Sacrificial Material. *Journal of Manufacturing Science and Engineering* 136 (6). 061014-061014-9.
[186] Leuders S, Lieneke T, Lammers S, Tröster T, Niendorf T (2014) On the Fatigue Properties of Metals Manufactured by Selective Laser Melting—The Role of Ductility. *Journal of Materials Research* 29:1911–1919.

[187] Leuders S, Thöne M, Riemer A, Niendorf T, Tröster T, Richard HA, Maier HJ (2013) O N the Mechanical Behaviour of Titanium Alloy TiAl6V4 Manufactured by Selective Laser Melting: Fatigue Resistance and Crack Growth Performance. *International Journal of Fatigue* 48:300–307.

[188] Levy GN, Schindel R, Kruth J-P (2003) Rapid Manufacturing and Rapid Tooling with Layer Manufacturing (LM) Technologies, State of the Art and Future Perspectives. *CIRP Annals Manufacturing Technology* 52(2):589–609.

[189] Lewis JA, Smay JE, Stuecker J, Cesarano J (2006) Direct Ink Writing of Three-dimensional Ceramic Structures. *Journal of the American Ceramic Society* 89 (12):3599–3609.

[190] Leyden RN, Messe L, Tran F, Johnson DI, Fong JW, Chapelat C, Patel RC (2012) Photocurable compositions for preparing ABS-like articles, US Patent 8,227,048.

[191] Li A, Thornton AS, Deuser B, Watts JL, Leu MC, Hilmas GE, Landers RG (2012) Freeze-form Extrusion Fabrication of Functionally Graded Material Composites Using Zirconium Carbide and Tungsten. *Proceedings of SFF Symposium*, Austin TX USA, 467–479.

[192] Li C, Fu CH, Guo YB, Fang FZ (2015) Fast Prediction and Validation of Part Distortion in Selective Laser Melting. *Procedia Manufacturing* 1:355–365.

[193] Li J, Monaghan T, Masurtschak S, Bournias-Varotsis A, Friel RJ, Harris RA (2015) Exploring the Mechanical Strength of Additively Manufactured Metal Structures with Embedded Electrical Materials. *Materials Science and Engineering A* 639:474–481.

[194] Li M, Tang L, Landers RG, Leu MC (2013) Extrusion Process Modeling for Aqueous-based Ceramic Pastes, Part 1: Constitutive Model. *Journal of Manufacturing Science and Engineering* 135(5). 051008-051008-7.

[195] Li M, Tang L, Landers RG, Leu MC (2013) Extrusion Process Modeling for Aqueous-based Ceramic Pastes—part 2: Experimental Verification. *Journal of Manufacturing Science and Engineering* 135(5). 051009-051009-7.

[196] Li P, Warner DH, Fatemi A, Phan N (2016) On the Fatigue Performance of Additively Manufactured Ti–6Al–4V to Enable Rapid Qualification for Aerospace Applications Traditionally Manufactured Ti–6Al–4V Reference Data. *57th AIAA/ASCE/AHS/ASC Structures, Structural Dynamics, and Materials Conference*, San Diego CA, 1–19.

[197] Li R, Liu J, Shi Y, Wang L, Jiang W (2012) Balling Behavior of Stainless Steel and Nickel Powder During Selective Laser Melting Process. *International Journal of Advanced Manufacturing Technology* 59:1025–1035.

[198] Li S, Wei Q, Shi Y, Zhu Z, Zhang D (2015) Microstructure Characteristics of Inconel 625 Superalloy Manufactured by Selective Laser Melting. *Journal of Materials Science & Technology* 31:946–952.

[199] Lin D, Jin S, Zhang F, Wang C, Wang Y, Zhou C, Cheng GJ (2015) 3D Stereolithography Printing of Graphene Oxide Reinforced Complex Architectures. *Nanotechnology* 26(43):434003.

[200] Liu D, Zhuang J, Shuai C, Peng S (2013) Mechanical Properties' Improvement of a Tricalcium Phosphate Scaffold with Poly-L-lactic Acid in Selective Laser Sintering. *Biofabrication* 5(2):025005.

[201] Liu F-H, Shen H-K, Liao Y-S (2011) Selective Laser Gelation of Ceramic–matrix Composites. *Composites Part B: Engineering* 42(1):57–61.

[202] Liu Q, Leu MC, Jose H, Richards VL (2004) Study of Ceramic Slurries for Investment Casting with Ice Patterns. *Proceedings of SFF Symposium*, Austin TX USA, 602–611.

[203] Louvis E, Fox P, Sutcliffe CJ (2011) Selective Laser Melting of Aluminium Components. *Journal of Materials Processing Technology* 211(2):275–284.

[204] Luo J, Gilbert LJ, Qu C, Morrow B, Bristow DA, Landers RG, Goldstein J, Urbas A, Kinzel EC (2015) Solid Freeform Fabrication of Transparent Fused Quartz Using a Filament Fed Process. *Proceedings of SFF Symposium*, Austin TX USA, 122–133.

[205] Ma M, Wang Z, Wang D, Zeng X (2013) Control of Shape and Performance for Direct Laser Fabrication of Precision Large-scale Metal Parts With 316L Stainless Steel. *Optics & Laser Technology* 45#1:209–216.

[206] MacKenzie K (1950) The Elastic Constants of a Solid Containing Spherical Holes. *Proceedings of the Physical Society* B63:2–11.

[207] Maeda K, Childs THC (2004) Laser Sintering (SLS) of Hard Metal Powders for Abrasion Resistant Coatings. *Journal of Materials Processing Technology* 149:609–615.

[208] Mansour S, Gilbert M, Hague R (2007) A Study of the Impact of Short-term Ageing on the Mechanical Properties of a Stereolithography Resin. *Material Science and Engineering A* 447(1–2):277–284.

[209] MarkForged, Markforged mechanical properties [datasheet], 11 May 2015. Retrieved from https://markforged.com/materials/, (August 2015).

[210] Maskery I, Aboulkhair N, Corfield M, Tuck C, Clare A, Leach R, Wildman R, Ashcroft I, Hague R (2016) Quantification and Characterisation of Porosity in Selectively Laser Melted Al–Si10–Mg Using X-ray Computed Tomography. *Materials Characterization* 111:193–204.

[211] McIntosh J, Danforth S, Jamalabad V (1997) Shrinkage and Deformation in Components Manufactured by Fused Deposition of Ceramics. *Proceedings of SFF Symposium*, Austin TX USA, 159–166.

[212] McMillen D, Li W, Leu MC, Hilmas GE, Watts J (2016) Designed Extrudate for Additive Manufacturing of Zirconium Diboride by Ceramic-on-demand Extrusion. *Proceedings of the SFF Symposium*, Austin, TX, 929–938.

[213] McNulty TF, Shanefield DJ, Danforth SC, Safari A (1999) Dispersion of Lead Zirconate Titanate for Fused Deposition of Ceramics. *Journal of the American Ceramic Society* 82:1757–1760.

[214] Melchels FPW, Feijen J, Grijpma DW (2010) A Review on Stereolithography and Its Applications in Biomedical Engineering. *Biomaterials* 31:6121–6130.

[215] Mercelis P, Kruth J-P (2006) Residual Stresses in Selective Laser Sintering and Selective Laser Melting. *Rapid Prototyping Journal* 12:254–265.

[216] Messe L, Chapelat C (2013) Curable Composition, US Patent 8,362,148.

[217] Meyers S, Kruth J-P, Vleugels J (2015) Direct Selective Laser Sintering of Reaction Bonded Silicon Carbide. *Proceedings of SFF Symposium*, Austin TX USA, 1750–1758.

[218] Montero Sistiaga ML, Mertens R, Vrancken B, Wang X, Van Hooreweder B, Kruth J-P, Van Humbeeck J (2016) Changing the Alloy Composition of Al7075 for Better Processability by Selective Laser Melting. *Journal of Materials Processing Technology* 238:437–445.

[219] Moore JP, Williams CB (2012) Fatigue Characterization of 3D Printed Elastomer Material. *Proceedings of the SFF Symposium*, Austin TX USA, 641–655.

[220] Mortensen A, Suresh S (1995) Functionally Graded Metals and Metal-ceramic Composites: Part 1 Processing. *International Materials Reviews* 40(6): 239–265.

[221] Mueller J, Shea K (2015) The Effect of Build Orientation on the Mechanical Properties in Inkjet 3D Printing. *Proceedings of SFF Symposium*, Austin TX USA, 983–992.

[222] Murr LE, Esquivel EV, Quinones SA, Gaytan SM, Lopez MI, Martinez EY, Medina F, Hernandez DH, Martinez E, Martinez JL, Stafford SW, Brown DK, Hoppe T, Meyers W, Lindhe U, Wicker RB (2009) Microstructures and Mechanical Properties of Electron Beam-Rapid Manufactured Ti–6Al–4V Biomedical Prototypes Compared to Wrought Ti–6Al–4V. *Materials Characterization* 60#2:96–105.

[223] Murr LE, Martinez E, Hernandez J, Collins S, Amato KN, Gaytan SM, Shindo PW (2012) Microstructures and Properties of 17-4 PH Stainless Steel Fabricated by Selective Laser Melting. *Journal of Materials Research and Technology* 1#3:167–177.

[224] Nag S, Samuel S, Puthucode A, Banerjee R (2009) Characterization of Novel Borides in Ti-Nb-Zr-Ta + 2B Metal–Matrix Composites. *Materials Characterization* 60(2):106–113.

[225] Napadensky E, Kritchman EM, Cohen A (2007) Compositions and methods for use in three dimensional model printing, US Patent 7,300,619.

[226] Ng CC, Savalani MM, Man HC, Gibson I (2010) Layer Manufacturing of Magnesium and Its Alloy Structures for Future Applications. *Virtual and Physical Prototyping* 5:13–19.

[227] Niendorf T, Leuders S, Riemer A, Richard H, Tröster T, Schwarze D (2013) Highly Anisotropic Steel Processed by Selective Laser Melting. *Metallurgical and Materials Transactions B* 44:794–796.

[228] Niino T, Uehara T (2015) Low Temperature Selective Laser Melting of High Temperature Plastic Powder. *Proceedings of the SFF Symposium*, Austin TX USA, 866–877.

[229] Niino T, Yamada H (2005) Transparentization of SLS Processed SMMA Copolymer Parts by Infiltrating a Thermosetting Epoxy Resin with Tuned Refractive index. *Proceedings of SFF Symposium*, Austin TX USA, 208–216.

[230] Niino T, Yamada H, Seki S (2004) Preliminary Study for Transparentization of SLS Parts by Resin Infiltration. *Proceedings of SFF Symposium*, Austin TX USA, 236–243.

[231] Niu FY, Wu DJ, Ma GY, Zhou SY, Zhang B (2014) Effect of Second-Phase Doping on Laser Deposited Al_2O_3 Ceramics. *Proceedings of the SFF Symposium*, Austin TX USA, 568–577.

[232] Niu FY, Wu DJ, Yan S, Ma GY, Zhang B (2017) Process optimization for suppressing cracks in laser engineered net shaping of Al_2O_3 ceramics. *JOM* 69(3):557–562.

[233] Olakanmi EO, Cochrane RF, Dalgarno KW (2015) A Review on Selective Laser Sintering/melting (SLS/SLM) of Aluminium Alloy Powders: Processing, Microstructure, and Properties. *Progress in Materials Science* 74:401–477.

[234] Olivier D, Borros S, Reyes G (2014) Application-Driven Methodology for New Additive Manufacturing Materials Development. *Rapid Prototyping Journal* 20 (1):50–58.

[235] Ottemer X, Colton JS (2002) Effects of Aging on Epoxy-Based Rapid Tooling Materials. *Rapid Prototyping Journal* 8(4):215–223.

[236] Pandey PM, Venkata Reddy N, Dhande SG (2003) Improvement of Surface Finish by Staircase Machining in Fused Deposition Modeling. *Journal of Materials Processing Technology* 132:323–331.

[237] Parimi LL, Ravi GA, Clark D, Attallah MM (2014) Microstructural and Texture Development in Direct Laser Fabricated IN718. *Materials Characterization* 89:102–111.

[238] Petch NJ (1953) The Cleavage Strength of Polycrystals. *Journal of the Iron and Steel Institute* 173:25–27.

[239] Peterkin FE, Stevens JL, Sharrow JF, Pitman RK (2003) High Voltage Breakdown Strength of Rapid Prototype Materials. *Proceedings of 14th IEEE International Pulsed Power Conference*, Dallas TX, 1025–1028.

[240] Pfister A, Landers R, Laib A, Hübner U, Schmelzeisen R, Mülhaupt R (2004) Biofunctional Rapid Prototyping for Tissue-Engineering Applications: 3D Bioplotting Versus 3D Printing. *Journal of Polymer Science Part A: Polymer Chemistry* 42:624–638.

[241] Pogson SR, Fox P, Sutcliffe CL, O'Neill W (2003) The Production of Copper Parts Using DMLR. *Rapid Prototyping Journal* 9:334–343.

[242] Pope MJ, Patterson MCL, Zimbeck W, Fehrenbacher M (1997) Laminated Object Manufacturing of Si_3N_4 with Enhanced Properties. *Proceedings of the SFF Symposium*, Austin TX USA, 529–536.

[243] Postiglione G, Natale G, Griffini G, Levi M, Turri S (2015) Conductive 3D Microstructures by Direct 3D Printing of Polymer/Carbon Nanotube Nanocomposites via Liquid Deposition Modeling. *Composites Part A: Applied Science and Manufacturing* 76:110–114.

[244] Puebla Arcaute KK, Quintana R, Wicker RB (2012) Effects of Environmental Conditions, Aging, and Build Orientations on the Mechanical Properties of ASTM Type I Specimens Manufactured via Stereolithography. *Rapid Prototyping Journal* 18(5):374–388.

[245] Puebla K, Murr LE, Gaytan SM, Martinez E, Medina F, Wicker RB (2012) Effect of Melt Scan Rate on Microstructure and Macrostructure for Electron Beam Melting of Ti–6Al–4V. *Materials Sciences and Applications* 3:259–264.

[246] Rafi HK, Karthik NV, Gong H, Starr TL, Stucker BE (2013) Microstructures and Mechanical Properties of Ti6Al4V Parts Fabricated by Selective Laser Melting and Electron Beam Melting. *Journal of Materials Engineering and Performance* 22#12:3872–3883.

[247] Ramazan AM, Majid TR, Hassan SB (2005) Heat Transfer Analysis of EDM Process on Silicon Carbide. *International Journal of Numerical Methods for Heat and Fluid Flow* 15(5):483–502.

[248] Ramirez D, Murr L, Martinez E, Hernandez D, Martinez J, Machado B, Medina F, Frigola P, Wicker R (2011) Novel Precipitate–Microstructural Architecture Developed in the Fabrication of Solid Copper Components by Additive Manufacturing Using Electron Beam Melting. *Acta Materialia* 59:4088–4099.

[249] Rangaswamy P, Griffith ML, Prime MB, Holden TM, Rogge RB, Edwards JM, Sebring RJ (2005) Residual Stresses in LENS® Components Using Neutron Diffraction and Contour Method. *Materials Science and Engineering: A* 399:72–83.

[250] Rickenbacher L, Etter T, Hövel S, Wegener K (2013) High Temperature Material Properties of IN738LC Processed by Selective Laser Melting (SLM) Technology. *Rapid Prototyping Journal* 19(4):282–290.

[251] Rieper H (2013) *Systematic Parameter Analysis for Selective Laser Melting (SLM) of Silver-Based Materials (MS Thesis)*, University of Louisville KY.

[252] Roberts CE, Bourell D, Watt T, Cohen J (2016) A Novel Processing Approach for Additive Manufacturing of Commercial Aluminum Alloys. *Physics Procedia* 83:909–917.

[253] Rocha CR, Perez ART, Roberson DA (2014) Novel ABS-Based Binary and Ternary Polymer Blends for Material Extrusion 3D Printing. *Journal of Materials Research* 29(17):1859–1866.

[254] Schmid M, Amado F, Levy G, Wegener K (2013) Flowability of Powders for Selective Laser Sintering (SLS) Investigated by Round Robin Test. *Proceedings of the 6th International Conference on Advanced Research in Virtual and Rapid Prototyping*, Leiria, Portugal, 95–99.

[255] Schmid M, Amado A, Wegener K (2014) Materials Perspective of Polymers for Additive Manufacturing with Selective Laser Sintering. *Journal of Materials Research* 29(17):1824–1832.

[256] Schmid M, Levy G (2009) Lasersintermaterialien—aktueller stand und entwicklungspotential. *fachtagung additive fertigung*, lehrstuhl für kunststofftechnik, Erlangen, Germany, 43–55.

[257] Schwendner KI, Banerjee R, Collins PC, Brice CA, Fraser HL (2001) Direct Laser Deposition of Alloys from Elemental Powder Blends. *Scripta Materialia* 45 (10):1123–1129.

[258] Sercombe TB, Schaffer GB (2003) Rapid Manufacturing of Aluminum Components. *Science* 301:1225–1227.

[259] Shahzad K, Deckers J, Boury S, Neirinck B, Kruth J-P, Vleugels J (2012) Preparation and Indirect Selective Laser Sintering of Alumina/PA Micro Spheres. *Ceramics International* 38(2):1241–1247.

[260] Simonelli M, Tse YY, Tuck C (2014) On the Texture Formation of Selective Laser Melted Ti–6Al–4V. *Metallurgical and Materials Transactions A* 45#6:2863–2872.

[261] Slocombe A, Li L (2001) Selective Laser Sintering of TiC–Al_2O_3 Composite with Self-Propagating High-Temperature Synthesis. *Journal of Materials Processing Technology* 118:173–178.

[262] Smay JE, Nadkarni SS, Xu J (2007) Direct Writing of Dielectric Ceramics and Base Metal Electrodes. *International Journal of Applied Ceramic Technology* 4 (1):47–52.

[263] Sperling LH (1981) *Interpenetrating Polymer Networks and Related Materials*, Plenum Press, New York.

[264] Sperling LH, Mishra V. (1996) in Salomone JC, (Ed.) *Polymer Materials Encyclopedia*, vol. 5. CRC Press, New York 3292.

[265] Spierings AB, Schoepf M, Kiesel R, Wegener K (2014) Optimization of SLM Productivity by Aligning 17-4PH Material Properties on Part Requirements. *Rapid Prototyping Journal* 20#6:444–448.

[266] Srivatsan TS, Manigandan K, Sudarshan TS (2015) Additive Manufacturing of Materials: Viable Techniques, Metals, Advances, Advantages, and Applications. *Additive Manufacturing*, CRC Press, Boca Raton FL1–48.

[267] Starr TL, Rafi K, Stucker B, Scherzer CM (2012) Controlling Phase Composition in Selective Laser Melted Stainless Steels. *Proceedings of the SFF Symposium*, Austin TX USA, 439–446.

[268] Steinmann B, Steinmann A (2005) Nanoparticle-filled stereolithographic resins, US Patent Application, US2005/0040562.

[269] Strano G, Hao L, Everson RM, Evans KE (2013) Surface Roughness Analysis, Modelling and Prediction in Selective Laser Melting. *Journal of Materials Processing Technology* 213:589–597.

[270] Suwanprateeb J, Sanngam R, Suvannapruk W, Panyathanmaporn T (2009) Mechanical and In Vitro Performance of Apatite–Wollastonite Glass Ceramic Reinforced Hydroxyapatite Composite Fabricated by 3D-printing. *Journal of Materials Science: Materials in Medicine* 20(6):1281–1289.

[271] Suwanprateeb F, Suwanpreuk W (2009) Development of Translucent and Strong Three Dimensional Printing Models. *Rapid Prototyping Journal* 15 (1):52–58.

[272] Svensson M (2011) Influence of Interstitials on Material Properties of TI6AL4V Fabricated with Electron Beam Melting (EBM®). *Medical Device Materials VI; Proceedings from the Materials & Processes for Medical Devices Conference*, ASM, International, Materials Park OH, 119–124.

[273] Syed WUH, Pinkerton AJ, Liu Z, Li L (2007) Coincident Wire and Powder Deposition by Laser to Form Compositionally Graded Material. *Surface and Coatings Technology* 201(16–17):7083–7091.

[274] Taghipour E, Leu MC, Guo N (2012) Comparison of Compression Molding and Selective Laser Sintering Processes in Development of Composite Bipolar Plates for Proton Exchange Membrane Fuel Cells. *Proceedings of SFF Symposium*, Austin TX USA, 226–237.

[275] Tammas-Williams S, Zhao H, Léonard F, Derguti F, Todd I, Prangnell PB (2015) XCT Analysis of the Influence of Melt Strategies on Defect Population in Ti–6Al–4V Components Manufactured by Selective Electron Beam Melting. *Materials Characterization* 102:47–61.

[276] Tan K, Chua C, Leong K, Cheah C, Cheang P, Abu Bakar M, Cha S (2003) Scaffold Development Using Selective Laser Sintering of Polyetheretherketone–Hydroxyapatite Biocomposite Blends. *Biomaterials* 24(18):3115–3123.

[277] Tang H-H (2006) Building Ultra-Thin Layers by Ceramic Laser Sintering. *Materials Transactions* 47(3):889–897.

[278] Thijs L (2014) *Microstructure and Texture of Metal Parts Produced by Selective Laser Melting (Doctoral Thesis)*, KU Leuven, Belgium.

[279] Thijs L, Kempen K, Kruth J-P, Van Humbeeck J (2013) Fine-Structured Aluminium Products with Controllable Texture by Selective Laser Melting of Pre-Alloyed AlSi10Mg Powder. *Acta Materialia* 61:1809–1819.

[280] Thijs L, Montero Sistiaga ML, Wauthle R, Xie Q, Kruth J-P, Van Humbeeck J (2013) Strong Morphological and Crystallographic Texture and Resulting Yield Strength Anisotropy in Selective Laser Melted Tantalum. *Acta Materialia* 61:4657–4668.

[281] Thijs L, Van Humbeeck J, Kempen K, Yasa E, Kruth J-P, Rombouts M (2011) Investigation on the Inclusions in Maraging Steel Produced by Selective Laser Melting. *Innovative Developments. Virtual and Physical Prototyping: Proceedings of the 5th International Conference on Advanced Research in Virtual and Rapid Prototyping*, Leiria, Portugal, CRC Press/Balkema, Leiden, The Netherlands, 297–304.

[282] Thijs L, Verhaeghe F, Craeghs T, Van Humbeeck J, Kruth J-P (2010) A Study of the Microstructural Evolution During Selective Laser Melting of Ti–6Al–4V. *Acta Materialia* 58#9:3303–3312.

[283] Thomas A, Kolan KCR, Leu MC, Hilmas GE (2015) Freeform Extrusion Fabrication of Titanium Fiber Reinforced Bioactive Glass Scaffolds. *Proceedings of SFF Symposium*, Austin TX USA, 1688–1699.

[284] Thompson MJ, Whalley DC, Hopkinson N (2008) Investigating Dielectric Properties of Sintered Polymers for Rapid Manufacturing. *Proceedings of SFF Symposium*, Austin TX USA, 79–93.

[285] Tolochko NK, Mozzharov SE, Yadroitsev IA, Laoui T, Froyen L, Titov VI, Ignatiev MB (2004) Balling Processes During Selective Laser Treatment of Powders. *Rapid Prototyping Journal* 10#2:78–87.

[286] Travitzky N, Bonet A, Dermeik B, Fey T, Filbert-Demut I, Schlier L, Schlordt T, Greil P (2014) Additive Manufacturing of Ceramic-Based Materials. *Advanced Engineering Materials* 16(6):729–754.

[287] Utela B, Storti D, Anderson R, Ganter M (2008) A Review of Process Development Steps for New Material Systems in Three Dimensional Printing (3DP). *Journal of Manufacturing Processes* 10:96–104.

[288] Utela BR, Storti D, Anderson RL, Ganter M (2010) Development Process for Custom Three-Dimensional Printing (3DP) Material Systems. *Journal of Manufacturing Science and Engineering* 132(1):110081–110089.

[289] Vaezi M, Chianrabutra S, Mellor B, Yang S (2013) Multiple Material Additive Manufacturing—Part 1: A Review. *Virtual and Physical Prototyping* 8(1):19–50.

[290] Vaezi M, Seitz H, Yang S (2012) A Review on 3d Microadditive Manufacturing Technologies. *International Journal of Advanced Manufacturing Technology* 67 (5-8):1721–1754.

[291] Van Hooreweder B, Moens D, Boonen R, Kruth J-P, Sas P (2012) Analysis of Fracture Toughness and Crack Propagation of Ti6Al4V Produced by Selective Laser Melting. *Advanced Engineering Materials* 14#1–2:92–97.

[292] Vandenbroucke B, Kruth J-P (2007) Selective Laser Melting of Biocompatible Metals for Rapid Manufacturing of Medical Parts. *Rapid Prototyping Journal* 13:196–203.

[293] Ventura SC, Narang SC, Sharma S, Stotts J, Liu C, Liu S, Ho L-H, Annavajjula D, Lombardi SJ, Hardy A, Mangaudis M, Chen E, Groseclose L (1996) A New SFF Process for Functional Ceramic Components. *Proceedings of SFF Symposium*, Austin TX USA, 327–334.

[294] Verbelen L (2016) *Towards Scientifically Based Screening Criteria for Polymer Laser Sintering (Doctoral Thesis)*, KU Leuven, Belgium.

[295] Verhaeghe F, Craeghs T, Heulens J, Pandelaers L (2009) A Pragmatic Model for Selective Laser Melting with Evaporation. *Acta Materialia* 57:6006–6012.

[296] Vilaro T, Colin C, Bartout JD (2011) As-Fabricated and Heat-Treated Microstructures of The Ti–6Al–4V Alloy Processed by Selective Laser Melting. *Metallurgical and Materials Transactions A* 42#10:3190–3199.

[297] Vitale A, Quaglio M, Chiodoni A, Bejtka K, Cocuzza M, Pirri CF, Bongiovanni R (2015) Oxygen-Inhibition Lithography for the Fabrication of Multipolymeric Structures. *Advanced Materials* 27:4560–4565.

[298] Vora P, Mumtaz K, Todd I, Hopkinson N (2015) AlSi12 In-Situ Alloy Formation and Residual Stress Reduction Using Anchorless Selective Laser Melting. *Additive Manufacturing* 7:12–19.

[299] Voxel8 (2015) *3D Printed Electronics, Bringing Functional Materials to 3D Printing*, http://www.voxel8.co/materials/.

[300] Vrancken B, Buls S, Kruth J-P, Van Humbeeck J (2015) Preheating of Selective Laser Melted Ti6Al4V-Microstructure and Mechanical Properties. *Proceedings of the World Conference on Titanium*, TMS, Warrendale PA, 1269–1277.

[301] Vrancken B, Thijs L, Kruth J-P, Van Humbeeck J (2012) Heat Treatment of Ti6Al4V Produced by Selective Laser Melting: Microstructure and Mechanical Properties. *Journal of Alloys and Compounds* 541:177–185.

[302] Vrancken B, Wauthlé R, Kruth J-P, Van Humbeeck J (2013) Study of the Influence of Material Properties on Residual Stress in Selective Laser Melting. *Proceedings of SFF Symposium*, Austin TX USA, 393–407.

[303] Wachtman JB, Cannon WR, Matthewson MJ (2009) Mechanical Properties of Whisker-, Ligament-, and Platelet-Reinforced Ceramic Matrix Composites. *Mechanical Properties of Ceramics*. 2nd ed. John Wiley & Sons, Inc, Hoboken, NJ277–289.

[304] Wang F, Mei J, Wu X (2008) Direct Laser Fabrication of Ti6Al4V/TiB. *Journal of Materials Processing Technology* 195(1–3):321–326.

[305] Wang T-M, Xi J-T, Jin Y (2007) A Model Research for Prototype Warp Deformation in the Fdm Process. *International Journal of Advanced Manufacturing Technology* 33:1087–1096.

[306] Wang Z, Denlinger E, Michaleris P, Stoica AD, Ma D, Beese AM (2017) Residual Stress Mapping in Inconel 625 Fabricated Through Additive Manufacturing: Method for Neutron Diffraction Measurements to Validate Thermomechanical Model Predictions. *Materials and Design* 117(5):169–177. http://dx.doi.org/10.1016/j.matdes.2016.10.003.

[307] Wang Z, Palmer TA, Beese AM (2016) Effect of Processing Parameters on Microstructure and Tensile Properties of Austenitic Stainless Steel 304L Made by Directed Energy Deposition Additive Manufacturing. *Acta Materialia* 110:226–235.
[308] Wei Q, Li S, Han C, Li W, Cheng L, Hao L, Shi Y (2015) Selective Laser Melting of Stainless-Steel/Nano-Hydroxyapatite Composites for Medical Applications: Microstructure, Element Distribution, Crack and Mechanical Properties. *Journal of Materials Processing Technology* 222:444–453.
[309] Weibull W (1951) A Statistical Distribution Function of Wide Applicability. *Journal of Applied Mechanics: Transactions ASME* 18(3):293–297.
[310] Weingarten C, Buchbinder D, Pirch N, Meiners W, Wissenbach K, Poprawe R (2015) Formation and Reduction of Hydrogen Porosity During Selective Laser Melting of AlSi10Mg. *Journal of Materials Processing Technology* 221:112–120.
[311] Wilkes J, Hagedorn Y-C, Meiners W, Wissenbach K (2013) Additive Manufacturing of ZrO_2-Al_2O_3 Ceramic Components by Selective Laser Melting. *Rapid Prototyping Journal* 19(1):51–57.
[312] Wilson JE (1974) *Radiation Chemistry of Monomers, Polymers, and Plastics*, Marcel Dekker, New York.
[313] Wiria FE, Leong KF, Chua CK, Liu Y (2007) Poly-ε-Caprolactone/Hydroxyapatite for Tissue Engineering Scaffold Fabrication via Selective Laser Sintering. *Acta Biomaterialia* 3(1):1–12.
[314] Wong KV, Hernandez A (2012) A Review of Additive Manufacturing. *ISRN Mechanical Engineering* 2012208760.
[315] Wu H, Li D, Guo N (2009) Fabrication of Integral Ceramic Mould for Investment Casting of Hollow Turbine Blade Based on Stereolithography. *Rapid Prototyping Journal* 15(4):232–237.
[316] Wu T, Das S (2011) Theoretical Modeling and Experimental Characterization of Stress Development in Parts Manufactured Through Large Area Maskless Photopolymerization. *Proceedings of SFF Symposium*, Austin TX USA, 748–760.
[317] Wudy K, Drummer D, Kühnlein F, Drexler M (2014) Influence of Degradation Behavior of Polyamide 12 Powders in Laser Sintering Process on Produced Parts. *AIP Conference Proceedings* 1593:691–695.
[318] Wycisk E, Emmelmann C, Siddique S, Walther F (2013) High Cycle Fatigue (HCF) Performance of Ti–6Al–4V Alloy Processed by Selective Laser Melting. *Advanced Materials Research* 816(817):134–139.
[319] Xin X-Z, Xiang N, Chen J, Xu D, Wei B (2012) Corrosion Characteristics of a Selective Laser Melted Co–Cr Dental Alloy under Physiological Conditions. *Journal of Materials Science* 47:4813–4820.
[320] Xiong Y, Smugeresky JE, Ajdelsztajn L, Schoenung JM (2008) Fabrication of WC-Co Cermets by Laser Engineered Net Shaping. *Materials Science and Engineering A* 493(1–2):261–266.
[321] Xu W, Brandt M, Sun S, Elambasseril J, Liu Q, Latham K, Xia K, Qian M (2015) Additive Manufacturing of Strong and Ductile Ti–6Al–4V by Selective Laser Melting via in Situ Martensite Decomposition. *Acta Materialia* 85:74–84.
[322] Xue Y, Pascu A, Horstemeyer MF, Wang L, Wang PT (2010) Microporosity Effects on Cyclic Plasticity and Fatigue of LENSTM-Processed Steel. *Acta Materialia* 58#11:4029–4038.
[323] Yadollahi A, Shamsaei N, Thompson SM, Elwany A, Bian L, Mahmoudi M (2015) Fatigue Behavior of Selective Laser Melted 17-4 PH Stainless Steel. *Proceedings of the SFF Symposium*, Austin TX USA, 721–731.
[324] Yadroitsev I, Pavlov M, Bertrand P, Smurov I (2009) Mechanical properties of samples fabricated by selective laser melting, 14èmes Assises Européennes du Prototypages & Fabrication Rapide, Paris.
[325] Yakovlev A, Trunova E, Grevey D, Pilloz M, Smurov I (2005) Laser-Assisted Direct Manufacturing of Functionally Graded 3D Objects. *Surface and Coatings Technology* 190:15–24.
[326] Yan L, Chen X, Li W, Newkirk J, Liou L (2016) Direct Laser Deposition of Ti–6Al–4V from Elemental Powder Blends. *Rapid Prototyping Journal* 22(5):810–816.
[327] Yang Y, Janaki Ram GD, Stucker BE (2007) An Experimental Determination of Optimum Processing Parameters For Al/SiC Metal Matrix Composites Made Using Ultrasonic Consolidation. *Journal of Engineering Materials and Technology* 129(4):538.
[328] Yasa E, Kruth J-P (2011) Microstructural Investigation of Selective Laser Melting 316L Stainless Steel Parts Exposed to Laser Re-Melting. *Procedia Engineering* 19:389–395.
[329] Yu J, Rombouts M, Maes G (2013) Cracking Behavior and Mechanical Properties of Austenitic Stainless Steel Parts Produced by Laser Metal Deposition. *Materials & Design* 45:228–235.
[330] Yu J, Rombouts M, Maes G, Motmans F (2012) Material Properties of Ti6Al4V Parts Produced by Laser Metal Deposition. *Physics Procedia* 39:416–424.
[331] Yu L-Y, Shen H-M, Xu Z-L (2009) PVDF–TiO_2 Composite Hollow Fiber Ultrafiltration Membranes Prepared by TiO_2 Sol–Gel Method and Blending Method. *Journal of Applied Physics* 113:1763–1772.
[332] Yuan M, Bourell D (2014) Additive Manufacturing of Optically Translucent Parts. *Proceedings of the SFF Symposium*, Austin TX USA, 865–874.
[333] Yuan M, Bourell D (2015) Optical Properties of Laser Sintered Polyamide 12. *Rapid Prototyping Journal* 21(4):443–448.
[334] Yuan M, Bourell D (2016) Orientation Effects for Laser Sintered Polyamide Optically Translucent Parts. *Rapid Prototyping Journal* 22(1):97–103.
[335] Yuan M, Bourell D (2016) Quality Improvement of Optically Translucent Parts Manufactured from LS and SL. *Rapid Prototyping Journal* 22(1):87–96.
[336] Zhang K, Wang S, Liu W, Shang X (2014) Characterization of Stainless Steel Parts by Laser Metal Deposition Shaping. *Materials & Design* 55:104–119.
[337] Zhang W, Leu MC, Ji Z, Yan Y (1998) Rapid Freezing Prototyping with Water. *Proceedings of SFF Symposium*, Austin TX USA, 185–192.
[338] Zhang XD, Zhang H, Grylls RJ, Lienert TJ, Brice C, Fraser HL, Keicher DM, Schlienger ME (2001) Laser-Deposited Advanced Materials. *Journal of Advanced Materials* 33#1:17–23.
[339] Zhang Y, Wei Z, Shi L, Xi M (2008) Characterization of Laser Powder Deposited Ti–TiC Composites and Functional Gradient Materials. *Journal of Materials Processing Technology* 206(1–3):438–444.
[340] Zhang YN, Cao X, Wanjara P, Medraj M (2013) Oxide Films in Laser Additive Manufactured Inconel 718. *Acta Materialia* 61:6562–6576.
[341] Zheng B, Smugeresky JE, Zhou Y, Baker D, Lavernia EJ (2008) Microstructure and Properties of Laser-Deposited Ti6Al4V Metal Matrix Composites Using Ni-Coated Powder. *Metallurgical and Materials Transactions A* 39A(5):1196–1205.
[342] Zheng B, Topping T, Smugeresky JE, Zhou Y, Biswas A, Baker D, Lavernia EJ (2010) The Influence of Ni-Coated TiC on Laser-Deposited IN625 Metal Matrix Composites. *Metallurgical and Materials Transactions A* 41(3):568–573.
[343] Zheng H, Zhang J, Lu S, Wang G, Xu Z (2006) Effect of Core–Shell Composite Particles on the Sintering Behavior and Properties of Nano-Al_2O_3/polystyrene Composite Prepared by SLS. *Materials Letters* 60(9–10):1219–1223.
[344] Ziemian CW, Cipoletti DE, Ziemian SN, Okwara MN, Haile KV (2014) Monotonic and Cyclic Tensile Properties of ABS Components Fabricated by Additive Manufacturing. *Proceedings of the SFF Symposium*, Austin TX USA, 525–541.
[345] Zito D, Carlotto A, Loggi A, Sbornicchia P, Maggian D, Unterberg P, Fockele M, Molinari A, Cristofolini I (2014) Optimization of SLM Technology Main Parameters in the Production of Gold and Platinum Jewelry. *Proceedings of the Santa Fe Symposium*, Albuquerque, NM, 1–24.
[346] Zocca A, Colombo P, Gomes CM, Günster J (2015) Additive Manufacturing of Ceramics: Issues, Potentialities, and Opportunities. *Journal of the American Ceramic Society* 98#7:1983–2001.